
Bayes Adaptive Monte Carlo Tree Search for Offline Model-based Reinforcement Learning

Jiayu Chen¹ Le Xu² Wentse Chen³ Jeff Schneider³

Abstract

Offline RL is a powerful approach for data-driven decision-making and control. Compared to model-free methods, offline model-based RL (MBRL) explicitly learns world models from a static dataset and uses them as surrogate simulators, improving the data efficiency and enabling the learned policy to potentially generalize beyond the dataset support. However, there could be various MDPs that behave identically on the offline dataset and dealing with the uncertainty about the true MDP can be challenging. In this paper, we propose modeling offline MBRL as a Bayes Adaptive Markov Decision Process (BAMDP), which is a principled framework for addressing model uncertainty. We further propose a novel Bayes Adaptive Monte-Carlo planning algorithm capable of solving BAMDPs in continuous state and action spaces with stochastic transitions. This planning process is based on Monte Carlo Tree Search and can be integrated into offline MBRL as a policy improvement operator in policy iteration. Our “RL + Search” framework follows in the footsteps of superhuman AIs like AlphaZero, improving on current offline MBRL methods by incorporating more computation input. The proposed algorithm significantly outperforms state-of-the-art offline RL methods on twelve D4RL MuJoCo tasks and three target tracking tasks in a challenging, stochastic tokamak control simulator. The codebase is available at: <https://github.com/LucasCJYSDL/Offline-RL-Kit>.

1. Introduction

The success of RL typically relies on large amounts of interactions with the environment. However, in real-world scenarios, such interactions can be unsafe or costly. As an alternative, offline RL (Levine et al., 2020; Chen et al., 2024a) leverages offline datasets of transitions, collected by a behavior policy, to train a policy. To avoid overestimation of the expected return for out-of-distribution states, which can mislead policy learning, model-free offline RL methods (Kumar et al., 2020; Wu et al., 2019) often constrain the learned policy to remain close to the behavior policy. However, acquiring a large volume of demonstrations from a high-quality behavior policy, can be expensive. This challenge has led to the development of offline model-based reinforcement learning (MBRL) approaches, such as (Lu et al., 2022; Guo et al., 2022). These methods train dynamics models from offline data and optimize policies using imaginary rollouts simulated by the models. Notably, the dynamics modeling is independent of the behavior policy, making it possible to learn effective policies even with data collected from a random policy. Further, with careful dynamics modeling and thorough simulation, the learned policy could potentially generalize to states beyond the support of the offline dataset.

Multiple MDPs can exhibit identical behaviors on an offline dataset of states and actions, yet their underlying dynamics and reward functions may differ, particularly on out-of-sample regions. This implies that we are dealing with a distribution of possible world models underlying a dataset. A common strategy in offline MBRL is to learn an ensemble of world models and treat them equally. For instance, when determining the next state, a world model would be uniformly sampled from the ensemble to generate its prediction. However, different ensemble members may perform better in different regions of the state-action space, making it necessary to adapt the belief over each ensemble member based on the experience. The Bayes Adaptive Markov Decision Process (BAMDP) (Duff, 2002) provides a principled framework for modeling such adaptations, and BAMCP (Guez et al., 2013) is an efficient online planning method for solving BAMDPs. However, BAMCP has several limitations: (1) it relies on a ground-truth world model

¹The University of Hong Kong, Hong Kong SAR ²Tsinghua University, Beijing, China, 100190 ³Carnegie Mellon University, PA 15213, USA. Correspondence to: Jiayu Chen <jia-yuc@hku.hk>.

for planning; (2) it is restricted to discrete state and action spaces; and (3) its outcome is an action choice at a particular state, rather than a policy function. To address these challenges: (1) we learn an ensemble of world models from the offline dataset and construct a pessimistic BAMDP atop of it as an estimation of the true MDP; (2) we propose a novel planning algorithm to solve BAMDPs in continuous state and action spaces based on double progressive widening (Auger et al., 2013); and (3) we integrate the planning component as a policy improvement operator within the policy iteration framework (Sutton & Barto, 2018), enabling the derivation of a policy function for real-time execution. Specifically, we conduct Monte Carlo Tree Search on a BAMDP as the planning process. Grounded in the scaling law, this paradigm of “RL+Search” has seen tremendous success in sophisticated policy learning, as demonstrated in (Silver et al., 2017b; AlphaProof & AlphaGeometry, 2024; Chen et al., 2023b). Its application to offline MBRL, particularly in continuous control tasks, remains a significant open challenge.

Our main contributions include: (1) Firstly using BAMDPs to handle model uncertainties in offline MBRL; (2) Proposing Bayes Adaptive Monte Carlo Tree Search for planning in continuous, stochastic BAMDPs; (3) Developing the first algorithm to successfully integrate Bayesian RL, offline MBRL, and deep search for data-driven continuous control; (4) Demonstrating the improvements brought by Bayesian RL and deep search across twelve D4RL MuJoCo tasks and three target tracking tasks in tokamak control (for nuclear fusion), highlighting the potential of our algorithm to tackle challenging, real-world problems.

2. Background

An MDP (Puterman, 2014) can be described as a tuple $\mathcal{M} = \langle \mathcal{S}, \mathcal{A}, \mathcal{P}, \mathcal{R}, \gamma \rangle$. \mathcal{S} and \mathcal{A} are the state space and action space, respectively. $\mathcal{P} : \mathcal{S} \times \mathcal{A} \rightarrow \Delta_{\mathcal{S}}$ is the dynamics function and $\mathcal{R} : \mathcal{S} \times \mathcal{A} \rightarrow \Delta_{[0,1]}$ is the reward function, where $\Delta_{\mathcal{X}}$ denotes the set of probability distributions on \mathcal{X} . $\gamma \in [0, 1)$ is a discount factor. A Bayes Adaptive MDP (BAMDP) (Duff, 2002) can model scenarios where the precise MDP $\mathcal{M}_{\theta} = \langle \mathcal{S}, \mathcal{A}, \mathcal{P}_{\theta}, \mathcal{R}_{\theta}, \gamma \rangle$ is uncertain but is known to follow a prior distribution $b_0(\theta)$. During planning, a Bayes-optimal agent would update its belief over the MDP based on its experience. Formally, a BAMDP can be described as a tuple $\mathcal{M}^+ = \langle \mathcal{S}^+, \mathcal{A}, \mathcal{P}^+, \mathcal{R}^+, \gamma \rangle$. \mathcal{S}^+ denotes the space of information states (s, b) , which is a composition of the physical state and the current belief over the MDP. After each transition (s, a, r, s') , the belief is updated to the corresponding Bayesian posterior: $b'(b) \propto b(b)P((s, a, r, s')|\theta) = b(b)\mathcal{P}_{\theta}(s'|s, a)\mathcal{R}_{\theta}(r|s, a)$.

Accordingly, \mathcal{P}^+ and \mathcal{R}^+ are defined as follows:

$$\begin{aligned} \mathcal{P}^+((s', b')|(s, b), a) &= \mathbb{1}(b' = b) \int_{\theta} \mathcal{P}_{\theta}(s'|s, a)b(\theta)d\theta \\ \mathcal{R}^+((s, b), a) &= \int_{\theta} \mathcal{R}_{\theta}(s, a)b(\theta)d\theta \end{aligned} \quad (1)$$

The Q-function that satisfies the Bellman optimality equations (i.e., Equation (2)) is the Bayes-optimal Q-function and $\pi^*(s, b) = \arg \max_a Q^*((s, b), a)$ is the Bayes-optimal policy. Actions derived from π^* are executed in the true MDP and constitute the best course of actions for a Bayesian agent with a prior belief b_0 over the underlying MDP (Guez et al., 2014). Bayesian RL (Ghavamzadeh et al., 2015) seeks to compute the optimal policy, π^* , and provides a principled framework for handling uncertainty in the world model \mathcal{M}_{θ} . However, the requirement for Bayesian posterior updates often renders it computationally intractable, and we discuss several approximate methods in Section 3.

$$\begin{aligned} Q^*(x, a) &= \mathcal{R}^+(x, a) + \gamma \int_{x'} V^*(x')\mathcal{P}^+(x'|x, a)dx' \\ V^*(x') &= \max_a Q^*(x', a), \forall x = (s, b) \in \mathcal{S}^+, a \in \mathcal{A} \end{aligned} \quad (2)$$

3. Related Works

Offline model-based RL: Offline RL (Chen et al., 2024b) enables an agent to learn control policies from datasets of environment transitions pre-collected by a behavior policy μ , i.e., $\mathcal{D}_{\mu} = \{[(s_t^i, a_t^i, r_t^i)]_{i=1}^N\}$. Offline Model-based RL (MBRL) methods explicitly learn world models \mathcal{M}_{θ} from \mathcal{D}_{μ} and adopt \mathcal{M}_{θ} as a surrogate simulator, enabling the learned policy to possibly generalize to states beyond \mathcal{D}_{μ} . Both planning methods (Argenson & Dulac-Arnold, 2021; Zhan et al., 2022; Diehl et al., 2023) and RL methods (Yu et al., 2020; Kidambi et al., 2020; Lu et al., 2022) can be applied on top of the learned \mathcal{M}_{θ} to obtain a policy. However, since \mathcal{D}_{μ} may not span the entire state-action space, \mathcal{M}_{θ} is unlikely to be globally accurate. Learning/Planning without any safeguards against such model inaccuracy can yield poor results. In this case, the authors of (Yu et al., 2020; Kidambi et al., 2020; Lu et al., 2022) propose learning an ensemble of world models, using ensemble-based uncertainty estimations to construct a pessimistic MDP (P-MDP), and learning a near-optimal policy atop it. Ideally, for any policy, the performance in the real environment is lower-bounded by the performance in the corresponding P-MDP (with high probability), thus avoiding being overly optimistic about an inaccurate model. **Notably, none of these offline MBRL methods have modeled the problem as a BAMDP, even though Bayesian RL provides a principled framework for handling model uncertainty.**

Bayes-adaptive planning: Approximate methods for solving BAMDPs, such as (Asmuth et al., 2009; Sorg et al.,

2010; Castro & Precup, 2010; Asmuth & Littman, 2011; Wang et al., 2012; Guez et al., 2013; Slade et al., 2020) have been developed. As a representative work, BAMCP (Guez et al., 2013) adopts Monte-Carlo Tree Search (MCTS) (Browne et al., 2012) for Bayes-adaptive planning and is shown to converge in probability to a near Bayes-optimal policy at the root node of the search tree. **However, all these methods cannot be applied to large-scale MDPs with continuous state and action spaces.** Also, these planning algorithms are not designed for offline MBRL. Thus, how to incorporate search-based planning for policy improvement in RL and how to handle the inaccuracy of the learned world model during planning still require exploration.

To sum up, we introduce a Bayesian approach to offline MBRL and leverage tree search to enhance policy learning. There are related works in both directions. (1) (Dorfman et al., 2021; Choshen & Tamar, 2023) propose to model offline Meta RL as a BAMDP and learn a belief-conditioned policy capable of adapting to multiple tasks. (Ghosh et al., 2022) apply the BAMDP framework to model-free offline RL, arguing that optimal policies for offline RL should be adaptive to all observed transitions. Nevertheless, these works do not explore the Bayesian treatment of model-based RL. (2) Model-based planning results can be utilized to improve the sample efficiency of RL. For instance, (Feinberg et al., 2018) propose Model-based Value Expansion. It uses the learned world model to generate imaginary rollouts, providing a more accurate estimation of value function targets for online actor-critic training. This idea is later extended to the offline RL setting by (Jeong et al., 2023). However, they do not employ BAMDP for uncertainty treatment, and, compared to model-based rollouts, MCTS can offer more exhaustive exploration.

4. Methodology

In this section, we present a novel offline MBRL algorithm based on Bayes Adaptive MCTS. In Section 4.2, we propose a Bayes Adaptive planning method (i.e., Continuous BAMCP) that can be applied to stochastic continuous control tasks. Then, in Section 4.3, we present a search-based policy iteration framework, where the search results (from Continuous BAMCP) are distilled into policy and value networks for policy improvement/evaluation at each iteration. In this way, we integrate offline MBRL with Bayes Adaptive MCTS. Both components require the use of an ensemble of world models for either practical implementation or uncertainty quantification, as detailed in Section 4.1.

4.1. The Key Role of Deep Ensembles

Offline MBRL methods estimate world models \mathcal{M}_θ from a static dataset \mathcal{D}_μ , which would inevitably induce epistemic uncertainty about the identity of the true MDP \mathcal{M}^* . Specif-

ically, there could be various potential MDPs that behave identically on the limited set of states and actions in \mathcal{D}_μ , but their dynamics and reward functions may differ, especially on out-of-sample states and actions. Thus, we are actually dealing with a distribution of world models that follow a prior distribution $b_0(\theta) \triangleq P(\mathcal{M}_\theta|\mathcal{D}_\mu)$. As introduced in Section 2, Bayesian RL based on BAMDP is a principled framework for handling model uncertainty by explicitly including the belief over the models in its state representation. Essentially, the belief is updated with experience, providing a measure of how the models’ uncertainty has changed since the beginning of the episode. As a result, the agent can adjust its behavior upon receiving new information that reduces the epistemic uncertainty. Such an adaptive policy is necessary to act optimally in offline RL, as demonstrated in (Ghosh et al., 2022).

The idea of deep ensembles (Lakshminarayanan et al., 2017) is to train multiple deep neural networks as approximations of a function (for uncertainty quantification), each using a different weight initialization and optimized with a different mini-batch sequence. For offline MBRL, we can learn an ensemble of dynamics models $\{\mathcal{P}_\theta^1, \dots, \mathcal{P}_\theta^K\}$ and reward models $\{\mathcal{R}_\theta^1, \dots, \mathcal{R}_\theta^K\}$ ¹ from the dataset \mathcal{D}_μ by minimizing the following supervised learning loss: ($i = 1, \dots, K$)

$$\begin{aligned} \mathcal{L}(\mathcal{P}_\theta^i) &= -\mathbb{E}_{(s,a,s') \sim \mathcal{D}_\mu} [\log \mathcal{P}_\theta^i(s'|s,a)] \\ \mathcal{L}(\mathcal{R}_\theta^i) &= -\mathbb{E}_{(s,a,r) \sim \mathcal{D}_\mu} [\log \mathcal{R}_\theta^i(r|s,a)] \end{aligned} \quad (3)$$

$\{(\mathcal{P}_\theta^i, \mathcal{R}_\theta^i)_{i=1}^K\}$ can be viewed as a set of independent and identically distributed (IID) samples from the prior $P(\mathcal{M}_\theta|\mathcal{D}_\mu)$ and constitute a finite approximation of the space of world models. With such an ensemble, the belief over the world models can be converted to a mass function over a set of K items, where the i -th element denotes the probability of being in the MDP $(\mathcal{P}_\theta^i, \mathcal{R}_\theta^i)$. In this case, a reasonable prior distribution is $b_0(\theta) = [1/K, \dots, 1/K]$, since these models are IID prior samples. After receiving a transition (s, a, r, s') , the belief can be updated as follows:

$$b'(\theta)(i) \propto b(\theta)(i) \mathcal{P}_\theta^i(s'|s,a) \mathcal{R}_\theta^i(r|s,a), \quad i = 1, \dots, K \quad (4)$$

This update requires a single inference from each ensemble member, but can be parallelized for computational efficiency. Equation (4) is a practical implementation of the Bayesian posterior update based on deep ensembles, where $b(\theta)$, $b'(\theta)$, and $\mathcal{P}_\theta^i(s'|s,a) \mathcal{R}_\theta^i(r|s,a)$ denote the prior, posterior distributions, and likelihood, respectively. This simplified definition of $b(\theta)$ also enables efficient execution of transitions in Bayesian RL, as described in Equation (1).

The ensemble can also be used for uncertainty quantification in offline MBRL. As aforementioned, our algorithm relies

¹The reward and dynamics function $(\mathcal{R}_\theta^i, \mathcal{P}_\theta^i)$ are usually trained as a unified probabilistic model $\mathcal{N}(\mu_\theta^i, \sigma_\theta^i)$, since the reward r can be viewed as an element of the next state s' .

on thorough search on the learned world models. Without any constraints on the search process, the learned policy may overfit to an inaccurate model (by overestimating the expected return) and fail in the true MDP. **Although the agent could adapt its belief and follow more reliable ensemble members in the Bayesian RL framework, there could be regions in the state-action space where none of the members generalize well, as they are all learned from a static offline dataset.** A typical solution is to construct a P-MDP (see Section 3), which discourages the policy from regions where there is large discrepancy between the true and learned world models. We construct the P-MDP by using a penalized reward $\tilde{r}(s, a, r, b(\theta))$:

$$r - \lambda \sqrt{\sum_{i=1}^K b(\theta)(i)(\sigma_{\theta}^i(s, a)^2 + \mu_{\theta}^i(s, a)^2) - \mu_{\theta}(s, a)^2} \quad (5)$$

The reward penalty is weighted by a hyperparameter $\lambda > 0$ and corresponds to the standard deviation (std) of a mixture of Gaussian distributions, where μ_{θ}^i and σ_{θ}^i are the mean and std from the ensemble member i , $\mu_{\theta}(s, a) = \sum_{i=1}^K b(\theta)(i)\mu_{\theta}^i(s, a)$. This penalty design combines epistemic and aleatoric model uncertainty and has been shown to be successful at capturing errors in predicted dynamics².

4.2. Continuous BAMCP

BAMCP (Guez et al., 2013) has been successful in solving large-scale BAMDPs, as detailed in Appendix A, but it is limited to scenarios with discrete state and action spaces. In this subsection, we introduce a novel planning method to approximate the Bayes-optimal policy at a decision point (s, h) (h denotes the transition history that ends at s), which can be used to solve BAMDPs with continuous states/actions and stochastic transition kernels.

Double Progressive Widening (DPW): DPW (Couëtoux et al., 2011; Auger et al., 2013) is a technique to extend the use of MCTS to continuous state and action spaces. Instead of exploring all possible actions and next states, DPW maintains a finite list of options to search at each decision point, incrementally adding new options to the list based on the visitation counts of that decision point. To be specific, for a node (s, h) , a new action a is sampled (with the current policy π) and added to its children set $C((s, h))$, if $\lfloor N((s, h))^{\alpha} \rfloor \geq |C((s, h))|$, where $\alpha \in (0, 1)$ is a hyperparameter that controls the growth rate and N denotes the visitation counts of (s, h) . Otherwise, an action is selected from existing options in $C((s, h))$ according to the UCT (Kocsis

²In the original literature (Lu et al., 2022), where the penalty design is used, the ensemble is treated as a uniformly-weighted mixture model, i.e., $b(\theta)(i) = 1/K$, ($i = 1, \dots, K$), since their belief is not adaptive. Equation (5) fits into the Bayesian RL framework by adapting the belief $b(\theta)$, which is part of our novelty.

& Szepesvári, 2006) rule. Similarly, to handle the infinitely many possible state transitions in stochastic environments, a new next state s' is added to the children set $C((s, h), a)$ only if $\lfloor N((s, h), a)^{\beta} \rfloor \geq |C((s, h), a)|$ ($\beta \in (0, 1)$). Otherwise, the least visited child in $C((s, h), a)$ will be selected as the next state. **With DPW, the sets of possible actions or next states to explore are finite, allowing deep tree search as in discrete scenarios.** The more promising states and actions (with higher N) have more subsequent branches, thereby reducing corresponding estimation uncertainty.

Integration of DPW and BAMCP: Directly combining DPW and BAMCP (i.e., Algorithm 3) cannot solve BAMDPs with continuous state and action spaces. As introduced in Appendix A, BAMCP relies on root sampling, which samples dynamics functions only at the root node and follows a specific dynamics function throughout a simulation rollout. However, the rationale of root sampling (i.e., Lemma A.1) does not hold when applying DPW³. As an alternative design, Polynomial Upper Confidence Tree (PUCT) (Auger et al., 2013), built upon DPW, is a provably consistent planning method for solving MDPs with infinite-scale state and action spaces and highly stochastic transition dynamics. Thus, we propose casting BAMDPs into MDPs (i.e., \mathcal{M}^+ defined in Section 2) and solving them with PUCT. The pseudo code is shown as Algorithm 1. **As the number of simulations $E \rightarrow \infty$, PUCT can find a near-optimal solution of \mathcal{M}^+ (Auger et al., 2013), which is also a near Bayes-optimal solution for the true environment.**

Proposed algorithm – Continuous BAMCP: In Algorithm 1, each simulation follows a path from the root node to an unvisited node, utilizing progressive widening when sampling actions or next states, as detailed in the ACTIONPW and STATEPW procedures. Compared to PUCT, the main modifications include: (1) replacing $\langle \mathcal{S}, \mathcal{P}, \mathcal{R} \rangle$ in MDPs with their extended definitions in BAMDPs, i.e., $\langle \mathcal{S}^+, \mathcal{P}^+, \mathcal{R}^+ \rangle$, and (2) applying reward penalties to account for model uncertainty. To be specific, in STATEPW, r and s' are sampled from the distribution predicted by all ensemble members, which is a practical implementation of sampling from \mathcal{R}^+ and \mathcal{P}^+ as outlined in Eq. (1). After receiving the transition (s, a, r, s') , the belief vector $b(\theta)$ is updated to $b'(\theta)$ following Eq. (4), finishing the transition in \mathcal{S}^+ from $(s, b(\theta))$ to $(s', b'(\theta))$. The transition history h is then updated to $h' = hars'$. Secondly, in SIMULATE, a penalized reward \tilde{r} (i.e., Eq. (5)) is used, which can effectively mitigate overfitting to an inaccurate model, as discussed in Section 4.1.

Algorithm 1 can be used to approximate the Bayes-optimal policy at (s, h) , which is $\pi_{\text{ret}}(a|(s, h)) \propto N((s, h), a)$, $a \in$

³The last equality of Eq. (6) does not hold, since $\tilde{b}(\theta|has') \propto \tilde{b}(\theta|ha)\tilde{\mathcal{P}}_{\theta}(s'|s, a) \neq \tilde{b}(\theta|ha)\mathcal{P}_{\theta}(s'|s, a)$. $\tilde{\mathcal{P}}_{\theta}(s'|s, a)$ represents the distribution of next states when applying DPW, which differs from the true distribution $\mathcal{P}_{\theta}(s'|s, a)$, as dictated by the DPW rule.

Algorithm 1 Continuous BAMCP

```

Input:  $\pi, V, E, d_{\max}, \gamma, \alpha, \beta, \mathcal{P}_{\theta}^{1:K}, \mathcal{R}_{\theta}^{1:K}$ 
procedure SEARCH( $(s, h), b(\theta)$ )
  for  $e = 1 \dots E$  do
    SIMULATE( $(s, h), b(\theta), d_{\max}$ )
  end for
   $\pi_{\text{ret}}(a|(s, h)) \propto N((s, h), a), a \in C((s, h))$ 
   $v_{\text{ret}} = \sum_{a \in C((s, h))} \frac{N((s, h), a)}{N((s, h))} Q((s, h), a)$ 
  return  $\pi_{\text{ret}}, v_{\text{ret}}$ 
end procedure
procedure SIMULATE( $(s, h), b(\theta), d$ )
  if  $d == 0$  then return  $V((s, h))$ 
   $a \leftarrow \text{ACTIONPW}((s, h))$ 
   $r, s', b'(\theta) \leftarrow \text{STATEPW}((s, h), b(\theta), a)$ 
   $N((s, h)) += 1, N((s, h), a) += 1$ 
  if  $N((s, h)) > 1$  then
     $R \leftarrow \text{SIMULATE}((s', hars'), b'(\theta), d - 1)$ 
  else
     $R \leftarrow V((s', hars'))$ 
  end if
  Access  $\tilde{r}$  or calculate  $\tilde{r}$  using Eq. (5)
   $R \leftarrow \tilde{r} + \gamma R$ , cache  $\tilde{r}$ 
   $Q((s, h), a) += \frac{R - Q((s, h), a)}{N((s, h), a)}$ 
  return  $R$ 
end procedure

procedure ACTIONPW( $(s, h)$ )
  if first visit then  $C((s, h)) \leftarrow \emptyset$ 
  if  $\lfloor N((s, h))^{\alpha} \rfloor \geq |C((s, h))|$  then
     $a \sim \pi(\cdot|(s, h))$ 
     $C((s, h)) \leftarrow C((s, h)) \cup \{a\}$ 
     $N((s, h), a), Q((s, h), a) \leftarrow 0, 0$ 
  else
     $a \leftarrow \arg \max_{x \in C((s, h))} \tilde{Q}((s, h), x)$ 
  end if
  return  $a$ 
end procedure

procedure STATEPW( $(s, h), b(\theta), a$ )
  if first visit then  $C((s, h), a) \leftarrow \emptyset$ 
  if  $\lfloor N((s, h), a)^{\beta} \rfloor \geq |C((s, h), a)|$  then
     $r \sim \sum_{i=1}^K b(\theta)(i) \mathcal{R}_{\theta}^i(\cdot|s, a)$ 
     $s' \sim \sum_{i=1}^K b(\theta)(i) \mathcal{P}_{\theta}^i(\cdot|s, a)$ 
    Update  $b(\theta)$  to  $b'(\theta)$  using Eq. (4)
     $C((s, h), a) \leftarrow C((s, h), a) \cup \{(r, s', b'(\theta))\}$ 
     $N((s', hars')) \leftarrow 0$ 
  return  $r, s', b'(\theta)$ 
end if
return the least visited node in  $C((s, h), a)$ 
end procedure

```

$C((s, h))$ (Auger et al., 2013). However, we aim to solve the entire BAMDP offline, eliminating the need for anything beyond simple inference using the policy network during deployment. This necessitates a well-learned policy function at each decision point, but we cannot execute Algorithm 1 at every (s, h) due to the scale of the state space. Therefore, we integrate the planning algorithm into a policy iteration framework as introduced in the next subsection. In this case, π and V in Algorithm 1 denote the policy and value functions from the previous learning iteration⁴; while π_{ret} and v_{ret} are the improved policy and value estimates for specific decision points. As additional details, multiple terms (labeled in blue) in Algorithm 1 have alternative designs across different literatures, which we elaborate on in Appendix B.

4.3. Overall Framework: Search-based Policy Iteration

Now, we present how to integrate continuous BAMCP into policy improvement/evaluation in a policy iteration framework, to obtain a near Bayes-optimal policy, i.e., π , that can be directly referred to during execution. The pseudo code of the overall framework is shown as Algorithm 2.

⁴ π and V are functions of (s, h) because the states in BAMDPs include both s and the corresponding belief $b(\theta)$. $b(\theta)$ is recursively updated using the history h and is a function of h .

For efficiency, a learner and a number of actors execute in parallel, reading from and sending data to the replay buffer \mathcal{D} respectively. The actors update their copies of policy and value functions every E_l learner steps.

Each actor interacts with the learned world models to sample trajectory segments τ . The starting states of these segments are sampled from the provided dataset \mathcal{D}_{μ} . Notably: (1) the segment length H is kept short to minimize error accumulation when interacting with the learned world models; and (2) the prior $b(\theta)$ at a starting state s is obtained by performing the Bayesian posterior update (i.e., Eq. (4)) on the offline trajectory to which s belongs. These belief updates are reliable, as the offline trajectories are collected from the true environment. At each decision point (s, h) of the segment, a SEARCH procedure (defined in Algorithm 1) is executed. The search result π_{ret} is then used to indicate the action choice, i.e., $a \sim \pi_{\text{ret}}(\cdot|(s, h))$. As in STATEPW, the subsequent transition process follows a BAMDP, where $r \sim \mathcal{R}^+(\cdot|(s, h), a)$, $s' \sim \mathcal{P}^+(\cdot|(s, h), a)$, and the belief $b(\theta)$ is adapted with the new transition.

With the collected segments, π is trained to mimic the search result π_{ret} by minimizing a cross-entropy loss (i.e., $\mathcal{L}(\pi, \{(s, h, \pi_{\text{ret}})_i\}_{i=1}^B})$), while V is updated using standard temporal difference learning methods (e.g., SAC (Haarnoja

Algorithm 2 Search-based Policy Iteration

Input: $T, E_l, \mathcal{P}_\theta^{1:K}, \mathcal{R}_\theta^{1:K}$

 Initialize π and $V, \mathcal{D} \leftarrow \emptyset$
procedure LEARNER

 $e \leftarrow 0$
while true **do**
 $\{(s, h, \pi_{\text{ret}}, \tilde{r}, s', h')_{i=1}^B \sim \mathcal{D}$
 $\min_{\pi} \mathcal{L}(\pi, \{(s, h, \pi_{\text{ret}})_{i=1}^B\})$
 $\min_V \mathcal{L}^{\text{TD}}(V, \{(s, h, \tilde{r}, s', h')_{i=1}^B\})$
 $e += 1$

 Update π, V in ACTOR if $e \% E_l == 0$
end while
end procedure
 $\mathcal{L}(\pi, \{(s, h, \pi_{\text{ret}})_{i=1}^B\}) = - \sum_{((s, h), \pi_{\text{ret}})} \pi_{\text{ret}}^T \log \pi(\cdot | (s, h)) / B$
procedure ACTOR

while true **do**

 Sample s from $\mathcal{D}_\mu, h \leftarrow s, \tau \leftarrow []$

 Obtain the prior $b(\theta)$ at s
for $t = 1 \dots H$ **do**
 $\pi_{\text{ret}}, v_{\text{ret}} \leftarrow \text{SEARCH}((s, h), b(\theta))$
 $a \sim \pi_{\text{ret}}(\cdot | (s, h))$

 Acquire $r, s', b'(\theta)$ as in STATEPW

 Calculate \tilde{r} using Eq. (5)

 Append τ with $((s, h), \tilde{r}, \pi_{\text{ret}}, v_{\text{ret}})$
 $s, h, b(\theta) \leftarrow s', h, b'(\theta)$
end for
 $\mathcal{D} \leftarrow \mathcal{D} \cup \{\tau\}$
end while
end procedure

et al., 2018)) based on the sampled transitions.⁵ As noted in (Hubert et al., 2021), π_{ret} improves π at each decision point, so repeatedly applying continuous BAMCP to obtain π_{ret} and projecting the search results to the parameter space of π (through supervised learning) constitute a powerful improvement operator to iteratively enhance the policy π .

5. Evaluation

We would evaluate the effectiveness of each algorithm component and compare our algorithm against a variety of baselines on both standard benchmarks and real-world challenges. We aim to answer the following research questions: **(RQ1)** Would using BAMDP improve policy performance (by properly adapting the belief over the ensemble members)? **(RQ2)** Can the proposed search method, Continuous BAMCP, further enhance the performance? **(RQ3)** How can the search outcomes (i.e., π_{ret}) be effectively used for policy updates? **(RQ4)** Is it necessary to apply reward penalties to mitigate the overestimation issue? **(RQ5)** Does the proposed algorithm outperform other deep-search-based offline RL methods, such as MuZero and its variants? **(RQ6)** Can the proposed algorithm be applied to complex, real-world data-driven control tasks? We address the first four research questions in Section 5.1, **RQ5** in Section 5.2, and **RQ6** in Section 5.3. [Please refer to Appendix E for additional evaluation results.](#)

5.1. Benchmarking Results on D4RL MuJoCo Tasks

To evaluate the effectiveness of each component in our algorithm, we introduce three variants: (1) Following existing offline MBRL methods, **BA-MBRL** leverages learned world

⁵The search result v_{ret} can be used to construct the value target, but we didn't observe performance improvements from it.

models as surrogate simulators, applying reward penalties to collected transitions and using standard online RL algorithms (e.g., SAC) to learn a policy. It models the problem as a BAMDP (rather than an MDP), with environment transitions defined by Equations (1) and (4) and the reward penalty by Equation (5), and is designed to evaluate the effectiveness of **Bayesian RL**. (2) **BA-MCTS** builds on BA-MBRL by introducing Continuous BAMCP (Algorithm 1) to plan at decision points, rather than inferring directly from the policy, to generate trajectories for downstream SAC, demonstrating the impact of **deep search** on policy learning. (3) **BA-MCTS-SL**, described in Algorithm 2, replaces the policy learning algorithm in BA-MCTS (i.e., policy gradient methods as in SAC) with **supervised learning** (SL), so we can see which approach offers a more efficient policy update mechanism (based on the search result π_{ret}).

We first evaluate our algorithms on a widely-used continuous control benchmark for offline RL methods – D4RL MuJoCo (Fu et al., 2020). The evaluation results for three types of robotic agents, each with offline datasets of four different qualities, are presented in Table 1. (1) Compared to SOTA offline MBRL methods, our algorithms achieve superior performance on nine out of twelve tasks. In terms of average performance, BA-MBRL significantly outperforms the baselines, demonstrating the effectiveness of using BAMDPs to handle model uncertainties in offline MBRL and addressing **RQ1**. **Further, in Appendix E.1, we show that employing a Bayes-adaptive ensemble, instead of a uniform ensemble, improves the prediction likelihood for the provided offline trajectories and reduces the prediction errors in imaginary rollouts.** As illustrative examples of such performance improvement, Figure 3 tracks belief adaptation during an offline rollout and several imaginary rollouts. (2) Both BA-MCTS and BA-MCTS-SL further improve upon

Data Type	Environment	BA-MCTS-SL (ours)	BA-MCTS (ours)	BA-MBRL (ours)	Optimized	COMBO	MOREL	MOPO
random	HalfCheetah	29.20 ± 2.00	36.23 ± 1.04	32.76 ± 1.16	31.7	38.8	25.6	35.4
random	Hopper	33.83 ± 0.10	31.56 ± 0.12	31.47 ± 0.03	12.1	17.9	53.6	11.7
random	Walker2d	21.89 ± 0.07	21.59 ± 0.32	21.45 ± 0.53	21.7	7.0	37.3	13.6
medium	HalfCheetah	70.47 ± 3.52	75.84 ± 3.81	56.54 ± 5.20	45.7	54.2	42.1	42.3
medium	Hopper	97.75 ± 7.09	96.70 ± 14.0	98.25 ± 3.42	69.3	97.2	95.4	28.0
medium	Walker2d	82.24 ± 1.85	74.73 ± 3.25	75.41 ± 4.17	79.7	81.9	77.8	17.8
med-replay	HalfCheetah	61.16 ± 1.60	65.45 ± 0.81	62.50 ± 0.18	58.0	55.1	40.2	53.1
med-replay	Hopper	106.3 ± 0.13	101.8 ± 3.46	93.91 ± 4.25	90.8	89.5	93.6	67.5
med-replay	Walker2d	92.13 ± 5.13	95.06 ± 2.11	97.54 ± 1.93	65.8	56.0	49.8	39.0
med-expert	HalfCheetah	80.53 ± 6.63	76.16 ± 10.3	90.52 ± 4.13	104.2	90.0	53.3	63.3
med-expert	Hopper	112.2 ± 0.29	108.3 ± 0.22	107.8 ± 0.37	105.8	111.1	108.7	23.7
med-expert	Walker2d	107.7 ± 0.82	110.0 ± 1.74	84.71 ± 0.87	97.1	103.3	95.6	44.6
Average Score		74.62	74.45	71.06	65.16	66.83	64.42	36.67

Table 1. Comparisons between the proposed algorithms and SOTA offline MBRL methods on the D4RL benchmark suite. Each value represents the normalized score, as proposed in (Fu et al., 2020), of the policy trained by the corresponding algorithm. These scores are undiscounted returns normalized to approximately range between 0 and 100, where a score of 0 corresponds to a random policy and a score of 100 corresponds to an expert-level policy. For our algorithms, we report the average score of the final ten policy learning epochs and its standard deviation across three random seeds. Results in the last four columns are taken from the original papers (Lu et al., 2022; Yu et al., 2021; Kidambi et al., 2020; Yu et al., 2020), respectively.

BA-MBRL, highlighting the enhancement brought by deep search in policy learning, as related to **RQ2**. (3) For **RQ3**, BA-MCTS-SL performs similarly to BA-MCTS, validating the effectiveness of both policy update mechanisms (i.e., policy gradient methods and supervised learning). However, BA-MCTS-SL struggles on Walker2d, where a warm-up training phase (using BA-MBRL) is required to establish a good initial policy. On the other hand, the advantage of the SL-based policy update is evident in the training plots of our algorithms in Figure 4, where BA-MCTS-SL exhibits much smoother learning curves compared to the other two algorithms, indicating greater robustness in model selection. (4) **We further compare our algorithms with model-free offline policy learning methods, as shown in Appendix E.2.** The performance improvement is even greater than that over model-based methods, highlighting the necessity of model-based learning. Particularly, when data quality is low, merely mimicking or staying close to the behavior policy would result in an underperforming policy. (5) **To investigate RQ4, we provide an ablation study in Appendix E.3 to demonstrate the necessity of incorporating the reward penalty in offline MBRL to mitigate the overexploitation issue.** We also find that the SL-based policy update is less sensitive to model inaccuracies.

For fair comparisons and real-time execution, we do not perform test-time search and adopt the same policy architecture as the baselines, i.e., a feedforward neural network, rather than an RNN that incorporates transition history as input. These alternative designs have the potential to further improve our algorithms. For implementation, we build on the codebase of Optimized (Lu et al., 2022), which thoroughly explores design choices in offline MBRL, making minimal changes to the code and hyperparameter settings⁶. Therefore, we believe the performance improvements in Table

⁶The hyperparameter setups are provided in Appendix C.

1 stem from the Bayesian RL framework and deep search components. Our algorithm can be integrated with other advancements in offline MBRL, such as more accurate world model learning and improved uncertainty quantification for constructing P-MDPs. **To validate this, in Appendix E.4, we incorporate a reward penalty design proposed in (Sun et al., 2023) into BA-MCTS, achieving the best overall performance on D4RL MuJoCo comparing with the most SOTA offline model-based RL algorithms such as (Sun et al., 2023; Jeong et al., 2023).** All the results are reproducible using the provided codebase.

5.2. Comparison with MuZero-type Methods

MuZero also applies deep search to MBRL. To evaluate its performance on D4RL MuJoCo tasks and answer **RQ5**, we use the open-source implementation and hyperparameter configurations of Sampled EfficientZero (Ye et al., 2021) provided by LightZero (Niu et al., 2023). Benchmarking results from LightZero indicate that Sampled EfficientZero achieves the best performance on (online) MuJoCo locomotion tasks compared to other MuZero variants. To adapt Sampled EfficientZero for offline learning, we employ the reanalyse technique proposed by (Schrittwieser et al., 2021). **The evaluation results are presented in Figure 1.** For reference, the expert-level episodic returns (corresponding to scores of 100) for HalfCheetah, Hopper, and Walker2d are 12135, 3234.3, and 4592.3, respectively. As shown, the results are significantly worse compared to the performance of offline RL methods listed in Table 1, despite Sampled EfficientZero’s higher computational cost. **(In Appendix E.5, we provide a detailed comparison of the computational costs and algorithm design of our proposed algorithms and Sampled EfficientZero.)** Notably, both Sampled EfficientZero and BA-MCTS-SL rely on supervised learning for policy improvement. However, for continuous control tasks,

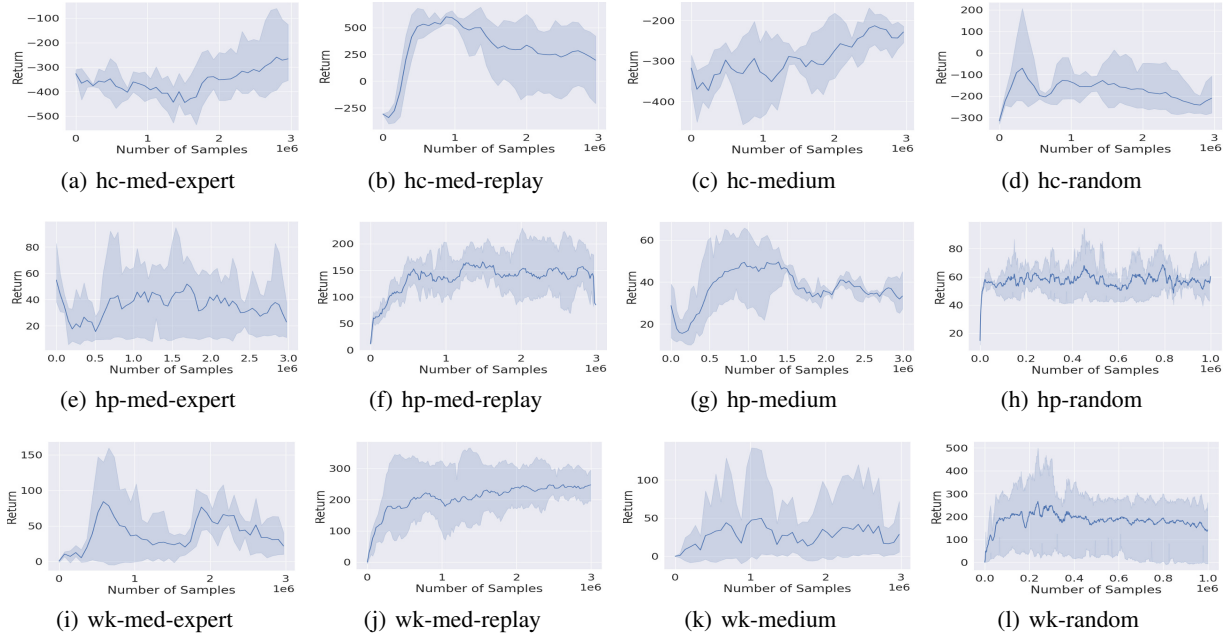


Figure 1. Performance of Sampled EfficientZero on D4RL MuJoCo tasks. The results for HalfCheetah, Hopper, and Walker2d are presented in the three rows, respectively. Each subfigure depicts the change in undiscounted episodic return as a function of the number of training samples. Experiments are repeated three times with different random seeds, with the solid line representing the mean and the shaded area indicating the 95% confidence interval. For reference, the expert-level episodic returns for HalfCheetah, Hopper, and Walker2d are 12135, 3234.3, and 4592.3, respectively.

the agent can only sample a finite number of actions at a decision point, and the search result (e.g., π_{ret} in Algorithm 1) is a distribution over this finite set, which could be a poor approximation of the optimal action distribution. Thus, purely mimicking the search result may be less sample-efficient than policy gradient methods, as it fails to account for the continuous nature of the action space. Further, world model learning is the foundation of MBRL and can be particularly challenging in continuous control and offline learning settings, where the state-action space is vast but training data is limited. Sampled EfficientZero integrates model learning and policy training into a single stage, which significantly increases the learning difficulty.

5.3. Applications to Tokamak Control

Finally, to investigate **RQ6**, we evaluate our algorithms on three target tracking tasks in tokamak control. The tokamak is one of the most promising confinement devices for achieving controllable nuclear fusion, where the primary challenge lies in confining the plasma, i.e., an ionized gas of hydrogen isotopes, while heating it and increasing its pressure to initiate and sustain fusion reactions (Pironti & Walker, 2005). Tokamak control involves applying a series of direct actuators (e.g., neutral beam, ECH power, magnetic field) and indirect actuators (e.g., setting targets for the plasma shape and density) to confine the plasma to achieve

a desired state or track a given target. This sophisticated physical process is an ideal test bed for our algorithms.

In particular, we use a well-trained data-driven dynamics model provided by (Char et al., 2024) as a “ground truth” simulator for the nuclear fusion process during evaluation, and generate a dataset (by this dynamics model) containing 725270 transitions for offline RL. We select a reference shot (i.e., an episode of a fusion process) from DIII-D⁷, and use its trajectories of Ion Rotation, Electron Temperature, and β_n as targets for three tracking tasks. These are critical quantities in tokamak control, particularly β_n , which serves as an economic indicator of the efficiency of nuclear fusion. The tracking tasks have a 28-dimensional state space and a 14-dimensional action space, both continuous. Moreover, these tasks are **highly stochastic**, as the underlying dynamics model is a probabilistic neural network and each state transition is a sample from this model. **For details on the simulator, and the design of the state/action spaces and reward functions, please refer to Appendix D.** We compare our algorithms with SOTA model-free and model-based offline RL methods, specifically CQL and Optimized. The learning performance on the three tracking tasks is shown in Figure 2, where the x-axis and y-axis represent the training

⁷DIII-D is a tokamak device located in San Diego, California, operated by General Atomics.

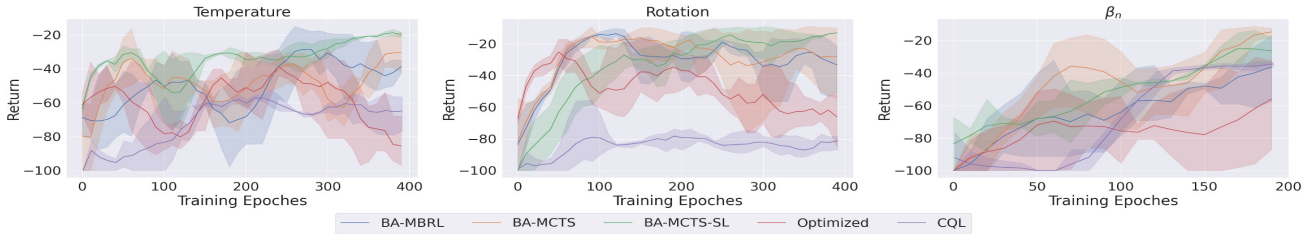


Figure 2. Evaluation results for the tokamak control tasks. The figure shows the change in episodic returns over training epochs for the proposed algorithms and baselines across three target tracking tasks in the nuclear fusion scenario. Solid lines represent the average performance, while shaded areas indicate the 95% confidence intervals.

Task	BA-MCTS-SL (ours)	BA-MCTS (ours)	BA-MBRL (ours)	CQL	Optimized
Temperature	-21.16 ± 5.00	-23.83 ± 9.66	-29.35 ± 4.72	-59.62 ± 1.57	-83.55 ± 10.56
Rotation	-14.14 ± 1.88	-19.07 ± 5.85	-31.33 ± 11.54	-85.48 ± 2.72	-71.54 ± 9.88
β_n	-37.03 ± 17.98	-18.93 ± 1.75	-23.4 ± 10.77	-36.37 ± 1.17	-57.84 ± 10.27
Average	-24.11	-20.61	-28.03	-60.49	-70.98

Table 2. Comparisons between the proposed algorithms and offline RL baselines on the target tracking tasks. For each algorithm, we report the average return of the final ten policy learning epochs and its standard deviation across three different random seeds.

epochs and (negative) full-shot tracking errors, respectively. Our algorithms consistently outperform the baselines. Notably, our algorithms share the same ensemble of dynamics models with “Optimized” for policy learning, and the comparisons can demonstrate the superiority of Bayesian RL and deep search. Figure 2 has been smoothed for visualization⁸. We further report the average return over the final 10 training epochs in Table 2, and the conclusions align with those from the D4RL MuJoCo tasks.

6. Conclusion and Discussions

In this work, we propose framing offline model-based reinforcement learning (MBRL) as a Bayes Adaptive Markov Decision Process (BAMDP) to better address uncertainties in the world models learned from offline datasets. We also introduce a novel planning method for solving BAMDPs in continuous state and action spaces using Monte Carlo Tree Search. This planning process is integrated into a policy iteration framework, enabling the derivation of a policy suitable for real-time execution from the planning results. In our evaluation, we test several variants of our algorithms to separately highlight the effectiveness of Bayesian RL and deep search. Additionally, we compare two different approaches for policy updates (based on the search results) in continuous control tasks: supervised learning and policy gradient methods. Our findings demonstrate that: (1) adapting beliefs over an ensemble of world models based on experience yields more accurate model approximations

⁸The episodic return is plotted every 10 epochs, with the y-axis being the average value of a sliding window of length 5.

for MBRL; (2) deep search improves learning performance by incorporating planning and additional computation input; and (3) while supervised-learning-based policy updates result in smoother learning curves, they may struggle in complex continuous control tasks due to their approximation of the continuous action space as a finite set of action samples. For future work, our algorithms can be further improved by integrating advancements in offline MBRL and Bayesian RL, such as Bayesian RL methods that do not rely on deep ensembles, techniques to address sparse rewards in MBRL, and more principled approaches to construct pessimistic MDPs beyond those based on ensemble discrepancy.

Acknowledgments

This work was funded in part by Department of Energy Fusion Energy Sciences under grant DE-SC0024544.

References

Abbate, J., Conlin, R., and Kolemen, E. Data-driven profile prediction for diii-d. *Nuclear Fusion*, 61(4):046027, 2021.

AlphaProof and AlphaGeometry. Ai achieves silver-medal standard solving international mathematical olympiad problems, 2024.

Antonoglou, I., Schrittwieser, J., Ozair, S., Hubert, T. K., and Silver, D. Planning in stochastic environments with a learned model. In *International Conference on Learning Representations*. OpenReview.net, 2022.

- Argenson, A. and Dulac-Arnold, G. Model-based offline planning. In *International Conference on Learning Representations*. OpenReview.net, 2021.
- Ariola, M., Pironti, A., et al. *Magnetic control of tokamak plasmas*, volume 187. Springer, 2008.
- Asmuth, J. and Littman, M. L. Approaching bayes-optimality using monte-carlo tree search. In *International Conference on Automated Planning and Scheduling*, 2011.
- Asmuth, J., Li, L., Littman, M. L., Nouri, A., and Wingate, D. A bayesian sampling approach to exploration in reinforcement learning. In *Uncertainty in Artificial Intelligence*, pp. 19–26. AUAI Press, 2009.
- Auger, D., Couëtoux, A., and Teytaud, O. Continuous upper confidence trees with polynomial exploration - consistency. In *European Conference on Machine Learning and Principles and Practice of Knowledge Discovery in Databases*, volume 8188, pp. 194–209. Springer, 2013.
- Browne, C. B., Powley, E., Whitehouse, D., Lucas, S. M., Cowling, P. I., Rohlfshagen, P., Tavener, S., Perez, D., Samothrakis, S., and Colton, S. A survey of monte carlo tree search methods. *IEEE Transactions on Computational Intelligence and AI in Games*, 4(1):1–43, 2012.
- Castro, P. S. and Precup, D. Smarter sampling in model-based bayesian reinforcement learning. In *Joint European Conference on Machine Learning and Knowledge Discovery in Databases*, volume 6321, pp. 200–214. Springer, 2010.
- Char, I., Abbate, J., Bardoczi, L., Boyer, M. D., Chung, Y., Conlin, R., Erickson, K., Mehta, V., Richner, N., Kolemén, E., and Schneider, J. G. Offline model-based reinforcement learning for tokamak control. In *Learning for Dynamics and Control Conference*, volume 211, pp. 1357–1372, 2023.
- Char, I., Chung, Y., Abbate, J., Kolemén, E., and Schneider, J. G. Full shot predictions for the DIII-D tokamak via deep recurrent networks. *CoRR*, abs/2404.12416, 2024.
- Chen, J., Aggarwal, V., and Lan, T. A unified algorithm framework for unsupervised discovery of skills based on determinantal point process. In *Advances in Neural Information Processing Systems*, 2023a.
- Chen, J., Lan, T., and Aggarwal, V. Hierarchical deep counterfactual regret minimization. *CoRR*, abs/2305.17327, 2023b.
- Chen, J., Ganguly, B., Lan, T., and Aggarwal, V. Variational offline multi-agent skill discovery. *CoRR*, abs/2405.16386, 2024a.
- Chen, J., Ganguly, B., Xu, Y., Mei, Y., Lan, T., and Aggarwal, V. Deep generative models for offline policy learning: Tutorial, survey, and perspectives on future directions. *Transactions on Machine Learning Research*, 2024b. ISSN 2835-8856.
- Chen, X., Yu, Y., Li, Q., Luo, F., Qin, Z. T., Shang, W., and Ye, J. Offline model-based adaptable policy learning. In *Advances in Neural Information Processing Systems*, pp. 8432–8443, 2021.
- Choshen, E. and Tamar, A. Contrabar: Contrastive bayes-adaptive deep RL. In *International Conference on Machine Learning*, volume 202, pp. 6005–6027. PMLR, 2023.
- Couëtoux, A., Hoock, J., Sokolovska, N., Teytaud, O., and Bonnard, N. Continuous upper confidence trees. In *International Conference on Learning and Intelligent Optimization*, volume 6683, pp. 433–445. Springer, 2011.
- Diehl, C., Sievernich, T., Krüger, M., Hoffmann, F., and Bertram, T. Uncertainty-aware model-based offline reinforcement learning for automated driving. *IEEE Robotics Automation Letters*, 8(2):1167–1174, 2023.
- Dorfman, R., Shenfeld, I., and Tamar, A. Offline meta reinforcement learning - identifiability challenges and effective data collection strategies. In *Advances in Neural Information Processing Systems*, pp. 4607–4618, 2021.
- Duff, M. O. *Optimal Learning: Computational procedures for Bayes-adaptive Markov decision processes*. University of Massachusetts Amherst, 2002.
- Feinberg, V., Wan, A., Stoica, I., Jordan, M. I., Gonzalez, J. E., and Levine, S. Model-based value expansion for efficient model-free reinforcement learning. In *International Conference on Machine Learning*, 2018.
- Fu, J., Kumar, A., Nachum, O., Tucker, G., and Levine, S. D4RL: datasets for deep data-driven reinforcement learning. *CoRR*, abs/2004.07219, 2020.
- Ghavamzadeh, M., Mannor, S., Pineau, J., and Tamar, A. Bayesian reinforcement learning: A survey. *Foundations and Trends® in Machine Learning*, 8(5-6):359–483, 2015.
- Ghosh, D., Ajay, A., Agrawal, P., and Levine, S. Offline RL policies should be trained to be adaptive. In *International Conference on Machine Learning*, volume 162, pp. 7513–7530. PMLR, 2022.
- Guez, A., Silver, D., and Dayan, P. Scalable and efficient bayes-adaptive reinforcement learning based on monte-carlo tree search. *Journal of Artificial Intelligence Research*, 48:841–883, 2013.

- Guez, A., Heess, N., Silver, D., and Dayan, P. Bayes-adaptive simulation-based search with value function approximation. In *Advances in Neural Information Processing Systems*, pp. 451–459, 2014.
- Guo, K., Shao, Y., and Geng, Y. Model-based offline reinforcement learning with pessimism-modulated dynamics belief. In *Advances in Neural Information Processing Systems*, 2022.
- Haarnoja, T., Zhou, A., Abbeel, P., and Levine, S. Soft actor-critic: Off-policy maximum entropy deep reinforcement learning with a stochastic actor. In *International Conference on Machine Learning*, volume 80, pp. 1856–1865. PMLR, 2018.
- Hamrick, J. B., Friesen, A. L., Behbahani, F. M. P., Guez, A., Viola, F., Witherspoon, S., Anthony, T., Buesing, L. H., Velickovic, P., and Weber, T. On the role of planning in model-based deep reinforcement learning. In *International Conference on Learning Representations*. OpenReview.net, 2021.
- Hubert, T., Schrittwieser, J., Antonoglou, I., Barekatin, M., Schmitt, S., and Silver, D. Learning and planning in complex action spaces. In *International Conference on Machine Learning*, volume 139 of *Proceedings of Machine Learning Research*, pp. 4476–4486. PMLR, 2021.
- Jeong, J., Wang, X., Gimelfarb, M., Kim, H., Abdulhai, B., and Sanner, S. Conservative bayesian model-based value expansion for offline policy optimization. In *International Conference on Learning Representations*. OpenReview.net, 2023.
- Kidambi, R., Rajeswaran, A., Netrapalli, P., and Joachims, T. Morel: Model-based offline reinforcement learning. In *Advances in Neural Information Processing Systems*, 2020.
- Kocsis, L. and Szepesvári, C. Bandit based monte-carlo planning. In *European Conference on Machine Learning*, volume 4212, pp. 282–293. Springer, 2006.
- Kumar, A., Fu, J., Soh, M., Tucker, G., and Levine, S. Stabilizing off-policy q-learning via bootstrapping error reduction. In *Advances in Neural Information Processing Systems*, pp. 11761–11771, 2019.
- Kumar, A., Zhou, A., Tucker, G., and Levine, S. Conservative q-learning for offline reinforcement learning. In *Advances in Neural Information Processing Systems*, 2020.
- Lakshminarayanan, B., Pritzel, A., and Blundell, C. Simple and scalable predictive uncertainty estimation using deep ensembles. In *Advances in Neural Information Processing Systems*, pp. 6402–6413, 2017.
- Lee, J., Jeon, W., Kim, G., and Kim, K. Monte-carlo tree search in continuous action spaces with value gradients. In *The Thirty-Fourth AAAI Conference on Artificial Intelligence*, pp. 4561–4568. AAAI Press, 2020.
- Levine, S., Kumar, A., Tucker, G., and Fu, J. Offline reinforcement learning: Tutorial, review, and perspectives on open problems. *CoRR*, abs/2005.01643, 2020.
- Liu, Z., Li, S., Lee, W. S., Yan, S., and Xu, Z. Efficient offline policy optimization with a learned model. In *International Conference on Learning Representations*. OpenReview.net, 2023.
- Lu, C., Ball, P. J., Parker-Holder, J., Osborne, M. A., and Roberts, S. J. Revisiting design choices in offline model based reinforcement learning. In *International Conference on Learning Representations*. OpenReview.net, 2022.
- Maćkiewicz, A. and Ratajczak, W. Principal components analysis (pca). *Computers & Geosciences*, 19(3):303–342, 1993.
- Niu, Y., Pu, Y., Yang, Z., Li, X., Zhou, T., Ren, J., Hu, S., Li, H., and Liu, Y. Lightzero: A unified benchmark for monte carlo tree search in general sequential decision scenarios. In *Advances in Neural Information Processing Systems*, 2023.
- Oren, Y., Spaan, M. T., and Böhrer, W. E-mcts: Deep exploration in model-based reinforcement learning by planning with epistemic uncertainty. *arXiv preprint arXiv:2210.13455*, 2022.
- Pironti, A. and Walker, M. Fusion, tokamaks, and plasma control: an introduction and tutorial. *IEEE Control Systems Magazine*, 25(5):30–43, 2005.
- Puterman, M. L. *Markov decision processes: discrete stochastic dynamic programming*. John Wiley & Sons, 2014.
- Rigter, M., Lacerda, B., and Hawes, N. RAMBO-RL: robust adversarial model-based offline reinforcement learning. In *Advances in Neural Information Processing Systems*, 2022.
- Schrittwieser, J., Antonoglou, I., Hubert, T., Simonyan, K., Sifre, L., Schmitt, S., Guez, A., Lockhart, E., Hassabis, D., Graepel, T., Lillicrap, T. P., and Silver, D. Mastering atari, go, chess and shogi by planning with a learned model. *Nature*, 588(7839):604–609, 2020.
- Schrittwieser, J., Hubert, T., Mandhane, A., Barekatin, M., Antonoglou, I., and Silver, D. Online and offline reinforcement learning by planning with a learned model. In *Advances in Neural Information Processing Systems*, pp. 27580–27591, 2021.

- Silver, D., Hubert, T., Schrittwieser, J., Antonoglou, I., Lai, M., Guez, A., Lanctot, M., Sifre, L., Kumaran, D., Graepel, T., Lillicrap, T. P., Simonyan, K., and Hassabis, D. Mastering chess and shogi by self-play with a general reinforcement learning algorithm. *CoRR*, abs/1712.01815, 2017a.
- Silver, D., Schrittwieser, J., Simonyan, K., Antonoglou, I., Huang, A., Guez, A., Hubert, T., Baker, L., Lai, M., Bolton, A., Chen, Y., Lillicrap, T. P., Hui, F., Sifre, L., van den Driessche, G., Graepel, T., and Hassabis, D. Mastering the game of go without human knowledge. *Nat.*, 550(7676):354–359, 2017b.
- Slade, P., Sunberg, Z. N., and Kochenderfer, M. J. Estimation and control using sampling-based bayesian reinforcement learning. *IET Cyber-Physical Systems: Theory & Applications*, 5(1):127–135, 2020.
- Sorg, J., Singh, S., and Lewis, R. L. Variance-based rewards for approximate bayesian reinforcement learning. In *Uncertainty in Artificial Intelligence*, pp. 564–571. AUAI Press, 2010.
- Sun, Y., Zhang, J., Jia, C., Lin, H., Ye, J., and Yu, Y. Model-bellman inconsistency for model-based offline reinforcement learning. In *International Conference on Machine Learning*, volume 202, pp. 33177–33194. PMLR, 2023.
- Sunberg, Z. N. and Kochenderfer, M. J. Online algorithms for pomdps with continuous state, action, and observation spaces. In *International Conference on Automated Planning and Scheduling*, pp. 259–263. AAAI Press, 2018.
- Sutton, R. S. and Barto, A. G. *Reinforcement Learning: An Introduction*. The MIT Press, second edition, 2018.
- Wang, Y., Won, K. S., Hsu, D., and Lee, W. S. Monte carlo bayesian reinforcement learning. In *International Conference on Machine Learning*, 2012.
- Wu, Y., Tucker, G., and Nachum, O. Behavior regularized offline reinforcement learning. *CoRR*, abs/1911.11361, 2019.
- Ye, W., Liu, S., Kurutach, T., Abbeel, P., and Gao, Y. Mastering atari games with limited data. In *Advances in Neural Information Processing Systems*, pp. 25476–25488, 2021.
- Yu, T., Thomas, G., Yu, L., Ermon, S., Zou, J. Y., Levine, S., Finn, C., and Ma, T. MOPO: model-based offline policy optimization. In *Advances in Neural Information Processing Systems*, 2020.
- Yu, T., Kumar, A., Rafailov, R., Rajeswaran, A., Levine, S., and Finn, C. COMBO: conservative offline model-based policy optimization. In *Advances in Neural Information Processing Systems*, pp. 28954–28967, 2021.
- Zhan, X., Zhu, X., and Xu, H. Model-based offline planning with trajectory pruning. In *International Joint Conference on Artificial Intelligence*, pp. 3716–3722. ijcai.org, 2022.
- Zhao, C., Niu, Y., Huang, K., Liu, Y., and Yuan, C. A perspective of improper dynamics on offline model-based planning, 2024. URL <https://openreview.net/forum?id=7kubdPr1RY>.

A. BAMCP

Algorithm 3 BAMCP

Input: $\pi, E, d_{\max}, \mathcal{R}, \gamma, \mathcal{A}, c$

```

procedure SEARCH( $(s, h), b(\theta)$ )
  for  $e = 1 \dots E$  do
     $\theta \sim b(\cdot)$ 
    SIMULATE( $(s, h), \theta, d_{\max}$ )
  end for
  return  $\arg \max_a Q((s, h), a)$ 
end procedure
    
```

```

procedure ROLLOUT( $(s, h), \theta, d$ )
  if  $d == 0$  then
    return 0
  end if
   $a \sim \pi(\cdot | (s, h))$ 
   $s' \sim \mathcal{P}_\theta(\cdot | s, a)$ 
   $r \leftarrow \mathcal{R}(s, a)$ 
   $R \leftarrow r + \gamma \text{ROLLOUT}((s', h), \theta, d - 1)$ 
  return  $R$ 
end procedure
    
```

```

procedure SIMULATE( $(s, h), \theta, d$ )
  if  $d == 0$  then
    return 0
  end if
  if  $N((s, h)) == 0$  then
    for  $a \in \mathcal{A}$  do
       $N((s, h), a), Q((s, h), a) \leftarrow 0, 0$ 
    end for
     $a \sim \pi(\cdot | (s, h))$ 
     $s' \sim \mathcal{P}_\theta(\cdot | s, a), r \leftarrow \mathcal{R}(s, a)$ 
     $R \leftarrow r + \gamma \text{ROLLOUT}((s', h), \theta, d - 1)$ 
     $N((s, h)), N((s, h), a) \leftarrow 1, 1$ 
     $Q((s, h), a) \leftarrow R$ 
    return  $R$ 
  end if
   $a \leftarrow \arg \max_x Q((s, h), x) + c \sqrt{\frac{\log N((s, h))}{N((s, h), x)}}$ 
   $s' \sim \mathcal{P}_\theta(\cdot | s, a), r \leftarrow \mathcal{R}(s, a)$ 
   $R \leftarrow r + \gamma \text{SIMULATE}((s', h), \theta, d - 1)$ 
   $N((s, h)) += 1, N((s, h), a) += 1$ 
   $Q((s, h), a) += \frac{R - Q((s, h), a)}{N((s, h), a)}$ 
  return  $R$ 
end procedure
    
```

Bayes Adaptive Monte Carlo Planning (BAMCP) (Guez et al., 2013) is a sample-based online planning method, aiming to find the action a^* that approximately maximizes the expected return at a decision point (s, h) under the BAMDP. Its detailed pseudo code is shown as Algorithm 3. BAMCP has demonstrated success in solving BAMDPs with large-scale **discrete** state and action spaces. Its key algorithmic ideas include: (1) applying MCTS with an efficient exploration strategy – UCT (Kocsis & Szepesvári, 2006) to the BAMDP in order to simulate the outcomes of different action choices; (2) utilizing root sampling to avoid frequent Bayesian posterior updates. Specifically, the UCT rule is used for selecting actions at non-leaf nodes, i.e., $a \leftarrow \arg \max_x Q((s, h), x) + c \sqrt{\frac{\log N((s, h))}{N((s, h), x)}}$, managing the tradeoff between exploration and exploitation. (As shown in Algorithm 3, N is the visit count, while Q denotes the accumulated reward.) Root sampling refers to sampling the dynamics model only at the root node (i.e., $\theta \sim b(\cdot)$) and not adapting the belief $b(\cdot)$ according to the Bayes rule and experience during the search process, of which the rationality is justified in the following lemma.

Lemma A.1. *For all suffix histories h' of h , $b(\theta|h') = \tilde{b}(\theta|h')$. Here, $b(\theta|h')$ is the true posterior probability of θ at the decision point h' , while $\tilde{b}(\theta|h')$ is the probability of experiencing θ at h' when using root sampling.*

Proof. This lemma can be proved by induction.

Base case: When $h' = h$, $b(\theta|h') = \tilde{b}(\theta|h') = b(\theta)$.

Step case:

$$\begin{aligned}
 b(\theta|has') &= P(has'|\theta)P(\theta)/P(has') \\
 &= P(h|\theta)\mathcal{P}_\theta(s'|s, a)P(\theta)/P(has') \\
 &= b(\theta|h)P(h)\mathcal{P}_\theta(s'|s, a)/P(has') \\
 &= Zb(\theta|h)\mathcal{P}_\theta(s'|s, a) \\
 &= Z\tilde{b}(\theta|h)\mathcal{P}_\theta(s'|s, a) \\
 &= Z\tilde{b}(\theta|ha)\mathcal{P}_\theta(s'|s, a) = \tilde{b}(\theta|has')
 \end{aligned} \tag{6}$$

Here, $Z = 1/\int_{\theta} \mathcal{P}_{\theta}(s'|s, a)b(\theta|h)d\theta = 1/\int_{\theta} \mathcal{P}_{\theta}(s'|s, a)\tilde{b}(\theta|h)d\theta = 1/\int_{\theta} \mathcal{P}_{\theta}(s'|s, a)\tilde{b}(\theta|ha)d\theta$ is the normalization constant. The fifth equality in Eq. (6) holds due to the inductive hypothesis. The sixth equality is based on the fact that the choice of a at each node h is made independently of the sample θ . As for the last equality, to experience θ at has' , the sample θ needs to traverse ha (with probability $\tilde{b}(\theta|ha)$) and then the state s' needs to be sampled, which is with probability $\mathcal{P}_{\theta}(s'|s, a)$, so $\tilde{b}(\theta|has') \propto \tilde{b}(\theta|ha)\mathcal{P}_{\theta}(s'|s, a)$. \square

B. Alternative Design Choices for Continuous BAMCP

The terms labeled in blue in Algorithm 1 have alternative design choices, which are introduced as below. Empirical comparisons among these alternatives are reserved for future work.

$\tilde{Q}((s, h), x)$ in the exploration strategy, i.e., $a \leftarrow \arg \max_{x \in C((s, h))} \tilde{Q}((s, h), x)$, could take various forms. For instance, in (Couëtoux et al., 2011; Guez et al., 2013; Lee et al., 2020), $\tilde{Q}((s, h), x) = Q((s, h), x) + c\sqrt{\frac{\log N((s, h))}{N((s, h), x)}}$; in PUCT (Auger et al., 2013), $\tilde{Q}((s, h), x) = Q((s, h), x) + \sqrt{\frac{N((s, h))e(d)}{N((s, h), x)}}$, where $e(d)$ is a schedule of coefficients related to the search depth d ; in Sampled MuZero (a variant of MuZero that can be applied in continuous action spaces (Hubert et al., 2021)), $\tilde{Q}((s, h), x) = Q((s, h), x) + \hat{\pi}(x|(s, h))\frac{\sqrt{N((s, h))}}{1+N((s, h), x)}\left(c_1 + \log\left(\frac{N((s, h))+c_2+1}{c_2}\right)\right)$. Here, c, c_1, c_2 are hyperparameters, $\hat{\pi} = \hat{\beta}\pi^{1-1/\tau}$ is a sample policy defined upon the real policy π . In particular, at each decision point (s, h) , Sampled MuZero would sample M actions $\{a_i\}$ from the distribution $\pi^{1/\tau}$ and accordingly define $\hat{\beta}(a|(s, h)) = \sum_i \mathbb{1}_{a_i=a}/M$, where $\tau > 0$ is a temperature hyperparameter. **Thus, Sampled MuZero does not adopt progressive widening like ours.** Following BAMCP, we adopt the first definition of $\tilde{Q}((s, h), x)$, though it could potentially be improved with other choices. In addition, as an implementation trick (Hamrick et al., 2021), the Q estimates are usually normalized into $\bar{Q} \in [0, 1]$ before being used to calculate \tilde{Q} as above. The normalized estimates can be computed as $\bar{Q}((s, h), x) = \frac{Q((s, h), x) - Q_{\min}}{Q_{\max} - Q_{\min}}$, where Q_{\max} and Q_{\min} are the maximum and minimum Q values observed in the search tree so far.

As the planning/search result, π_{ret} can take multiple forms. In (Guez et al., 2013; Sunberg & Kochenderfer, 2018; Lee et al., 2020), $\pi_{\text{ret}}((s, h)) = \arg \max_{a \in C((s, h))} Q((s, h), a)$; in (Sampled) MuZero, $\pi_{\text{ret}}(a|(s, h)) = \frac{N((s, h), a)^{1/\tau}}{\sum_{x \in C((s, h))} N((s, h), x)^{1/\tau}}$; in ROSMO (a variant of MuZero with improved performance in offline scenarios (Liu et al., 2023)), $\pi_{\text{ret}}(a|(s, h)) \propto \pi(a|(s, h)) \exp(Q((s, h), a) - V((s, h)))$. Here, $\tau \in (0, 1]$ is a temperature parameter and decays with the training process, ensuring the action selection becomes greedier. We select the second form for π_{ret} in Algorithm 1. This is because (1) as described in PUCT, the returned action should be the most visited one, which is not necessarily the one with the highest Q value, and (2) ROSMO adopts one-step look-ahead rather than deep tree search at each root node, which does not align with our approach.

As for the conditions of double progressive widening, PUCT designs α and β to be functions of the search depth d , while UCT-DPW (Couëtoux et al., 2011) utilizes a different set of conditions: $\lceil K_a N((s, h))^\alpha \rceil \geq |C((s, h))|$, $\lceil K_s N((s, h), a)^\beta \rceil \geq |C((s, h), a)|$, where K_a, K_s, α, β are all constant hyperparameters. Moreover, when the progressive widening condition for sampling the next state is not satisfied, either the least visited node in $C((s, h), a)$ can be selected (following PUCT), or a random node can be sampled from $C((s, h), a)$ according to a distribution proportional to the number of visits (following UCT-DPW). As shown in Algorithm 1, **we follow the designs of PUCT**, but keep α and β as constants for simplicity in hyperparameter fine-tuning.

Finally, the condition for continuing the simulation procedure, i.e., $N((s, h)) > 1$, could potentially be replaced with $N((s, h), a) > 1$ or $N((s', has')) > 0$. These conditions indicate that the nodes (s, h) , (s, h, a) , and (s', has') have been visited before, respectively. At the end of the simulation procedure, we can either apply rollouts, i.e., simulating a single path until the end of an episode, to estimate the expected value for a leaf node (s, h) , or directly use $V((s, h))$ as the estimation. The former approach is widely used in online planning algorithms (Guez et al., 2013; Sunberg & Kochenderfer, 2018; Lee et al., 2020; Chen et al., 2023a), while the latter is used in policy iteration frameworks like ours.

C. Key Hyperparameter Setup

In Table 3, we list the key hyperparameters of the proposed algorithms. **For each task, an ensemble of K dynamics and reward models is trained using the provided offline dataset. These learned models are then utilized as a simulator to train a control policy using off-the-shelf RL methods, such as SAC. The policy is trained for N epochs. At each**

Data Type	Environment	BA-MBRL				BA-MCTS				BA-MCTS-SL			
		K	λ	H	N	K	λ	H	N	K	λ	H	N
random	HalfCheetah	10	7	6	200	10	7	6	800	10	7	6	500
random	Hopper	6	50	47	700	6	50	47	800	6	50	47	500
random	Walker2d	10	0.5	20	700	10	0.5	20	800	10	0.5	20	500
medium	HalfCheetah	12	6	6	300	12	6	5	800	12	6	5	500
medium	Hopper	12	40	42	200	12	40	42	800	12	40	42	200
medium	Walker2d	8	5	20	700	8	5	20	800	8	5	20	500
med-replay	HalfCheetah	11	40	10	300	11	40	10	800	11	40	10	500
med-replay	Hopper	7	5	5	700	7	5	5	800	7	5	5	500
med-replay	Walker2d	13	2.5	47	1000	13	2.5	47	800	13	2.5	47	500
med-expert	HalfCheetah	7	100	5	1000	7	100	5	800	7	100	5	1100
med-expert	Hopper	12	40	43	600	12	40	43	800	12	40	43	500
med-expert	Walker2d	6	20	37	400	6	20	37	800	6	20	37	500

Table 3. Key hyperparameters of the proposed algorithms for each evaluation task. K : ensemble size, λ : reward penalty coefficient, H : rollout horizon, N : number of training epochs.

epoch, 50000H transitions are sampled by interacting with the simulator, followed by 1000 RL training iterations. In particular, 50000 states are randomly sampled from the offline dataset, with each state followed by a rollout lasting H time steps. To mitigate overestimation, a reward penalty based on the discrepancy among the ensemble members is applied with a coefficient λ , as shown in Equation (5). The setups for K , λ , and H are almost the same across the three algorithms and primarily inherited from the baseline – “Optimized” (Lu et al., 2022), to make sure the improvements are brought by the Bayesian RL and deep search components (rather than tricky hyperparameter setups).

The policy is evaluated on the ground truth environment for 10 episodes at the end of each training epoch. For all tables involving benchmarking results on D4RL, we report the average scores across the final 10 training epochs of our algorithms. It is important to note that increasing the number of training epochs N does not necessarily lead to better policy performance, since the training is based on learned dynamics and reward models rather than the ground truth. According to (Lu et al., 2022) and our experiments, the hyperparameters listed above can significantly influence the performance of model-based RL. Adjusting these hyperparameters could either enhance or impair the learning performance of our algorithms. We also suspect that the performance of the baselines listed in Tables 1 and 8, which are from their original papers, could be further improved by fine-tuning the relevant hyperparameters.

Data Type	Environment	BA-MCTS						BA-MCTS-SL							
		ρ	α	c	η	n_s	n_a	ρ	α	c	η	n_s	n_a	N_{SL}	N_P
random	HalfCheetah	0.1	0.5	2.5	0.3	1	20	0.1	0.5	2.5	0.3	1	20	5	0
random	Hopper	0.1	0.5	2.5	0.3	1	20	0.1	0.5	2.5	0.3	1	20	5	0
random	Walker2d	0.1	0.5	2.5	0.3	1	20	0.1	0.5	2.5	0.3	1	20	5	100
medium	HalfCheetah	0.1	0.5	1.0	0.1	5	10	0.1	0.5	1.0	0.1	5	10	20	0
medium	Hopper	0.1	0.5	2.5	0.3	1	20	0.1	0.5	1.0	0.3	1	20	5	0
medium	Walker2d	0.1	0.5	2.5	0.3	1	20	0.1	0.5	2.5	0.3	1	20	5	100
med-replay	HalfCheetah	0.1	0.8	1.0	0.3	5	10	0.1	0.8	2.5	0.3	1	20	5	0
med-replay	Hopper	0.1	0.8	1.0	0.1	1	20	0.1	0.8	1.0	0.1	1	20	15	0
med-replay	Walker2d	0.1	0.8	2.5	0.3	1	20	0.1	0.8	2.5	0.3	1	20	5	200
med-expert	HalfCheetah	0.1	0.8	1.0	0.3	5	10	0.1	0.8	2.5	0.3	1	20	5	0
med-expert	Hopper	0.1	0.8	1.0	0.3	1	20	0.1	0.8	1.0	0.3	1	20	5	0
med-expert	Walker2d	0.1	0.8	2.5	0.3	1	20	0.1	0.8	2.5	0.3	1	20	15	100

Table 4. Important hyperparameters used in the search process.

BA-MCTS and BA-MCTS-SL utilize Bayes Adaptive Monte Carlo Tree Search to collect samples for offline model-based RL. **Instead of performing a tree search at every state, we randomly select a proportion (i.e., ρ) of states from the available 50000 states at each rollout time step as root nodes for tree search to decide on the optimal actions. For the remaining states, actions are sampled directly from the policy, i.e., $a \sim \pi(\cdot|s)$.** The tree search procedure is detailed in Algorithm 1,

with the number of MCTS iterations, E , set to 50. **Increasing ρ and E can potentially enhance performance, but it will also linearly increase the computational cost.** Table 4 outlines the key hyperparameters related to the search process for each algorithm and task. (1) As described in Algorithm 1, the parameters α and β control the rate of double progressive widening. (β is set as 0.5 across all tasks.) To encourage deeper search, we limit the number of actions sampled from a state under n_a and the number of next states sampled from an action under n_s , respectively. Action selection follows the UCT rule, as discussed in Appendix A, where $c > 0$ balances the exploration and exploitation. Additionally, inspired by the success of MuZero in enhancing exploration, we introduce Dirichlet noise x_d at the root nodes, where actions are sampled from a mixture of distributions: $a \sim \eta x_d + (1 - \eta)\pi(\cdot|s)$ and η controls the mixture rate. Notably, for (c, η, n_a, n_s) , we explore the set of possible combinations: $\{(2.5, 0.3, 20, 1), (1.0, 0.3, 20, 1), (1.0, 0.1, 20, 1), (1.0, 0.3, 10, 5), (1.0, 0.1, 10, 5)\}$ during hyperparameter fine-tuning. We believe there are likely more optimal search settings yet to be discovered. (2) In BA-MCTS-SL, policy improvement is achieved through supervised learning. We find that, rather than learning solely from samples collected within the current epoch, incorporating a buffer of samples from the past N_{SL} epochs helps to stabilize the learning process. Also, in the Walker2d environment, BA-MCTS-SL requires a warm-up training phase of N_P epochs using BA-MBRL, allowing the initial policy to generate effective signals for supervised learning.

D. Details of the Tokamak Control Tasks

STATE SPACE	
Scalar States	β_n , Internal Inductance, Line Averaged Density, Loop Voltage, Stored Energy
Profile States	Electron Density, Electron Temperature, Pressure, Safety Factor, Ion Temperature, Ion Rotation
ACTION SPACE	
Targets	Current Target, Density Target
Shape Variables	Elongation, Top Triangularity, Bottom Triangularity, Minor Radius, Radius and Vertical Locations of the Plasma Center
Direct Actuators	Power Injected, Torque Injected, Total Deuterium Gas Injection, Total ECH Power, Magnitude and Sign of the Toroidal Magnetic Field

Table 5. The state and action spaces of the tokamak control tasks.

Nuclear fusion is a promising energy source to meet the world’s growing demand. It involves fusing the nuclei of two light atoms, such as hydrogen, to form a heavier nucleus, typically helium, releasing energy in the process. The primary challenge of fusion is confining a plasma, i.e., an ionized gas of hydrogen isotopes, while heating it and increasing its pressure to initiate and sustain fusion reactions. The tokamak is one of the most promising confinement devices. It uses magnetic fields acting on hydrogen atoms that have been ionized (given a charge) so that the magnetic fields can exert a force on the moving particles (Pironti & Walker, 2005).

(Char et al., 2024) trained a deep recurrent network as a dynamics model for the DIII-D tokamak, a device located in San Diego, California, and operated by General Atomics, using a large dataset of operational data from that device. A typical shot (i.e., episode) on DIII-D lasts around 6-8 seconds, consisting of a one-second ramp-up phase, a multi-second flat-top phase, and a one-second ramp-down phase. The DIII-D also features several real-time and post-shot diagnostics that measure the magnetic equilibrium and plasma parameters with high temporal resolution. **The authors demonstrate that the learned model predicts these measurements for entire shots with remarkable accuracy. Thus, we use this model as a “ground truth” simulator for tokamak control tasks. Specifically, we generate a dataset of 725270 transitions for offline RL and evaluate the learned policy using this data-driven simulator.**

The state and action spaces for the tokamak control tasks are outlined in Table 5. For detailed physical explanations of their components, please refer to (Abbate et al., 2021; Char et al., 2023; Ariola et al., 2008). The state space consists of five scalar values and six profiles which are discretized measurements of physical quantities along the minor radius of the toroid. After applying principal component analysis (Maćkiewicz & Ratajczak, 1993), the pressure profile is reduced to two dimensions, while the other profiles are reduced to four dimensions each. In total, the state space comprises 27 dimensions. The action space includes direct control actuators for neutral beam power, torque, gas, ECH power, current, and magnetic field, as well as target values for plasma density and plasma shape, which are managed through a lower-level

control module. Altogether, the action space consists of 14 dimensions. While for certain tasks, it is possible to prune the state and action spaces to reduce the learning complexity, we have chosen not to apply any domain-specific knowledge in these evaluations for general RL algorithms. We reserve the domain-specific applications of our algorithms, which would require more domain knowledge and engineering efforts, as an important future work.

We select a reference shot from DIII-D, which spans 251 time steps, and use its trajectories of Ion Rotation, Electron Temperature, and β_n as targets for three tracking tasks. Specifically, β_n is the normalized ratio between plasma pressure and magnetic pressure, a key quantity serving as a rough economic indicator of efficiency. Since the tracking targets vary over time, we include the time step as part of the policy input. The reward function for each task is defined as the negative squared tracking error of the corresponding component (i.e., temperature, rotation, or β_n) at each time step, and the reward is normalized by the episode horizon (i.e., 251 time steps). Notably, for policy learning, the reward function is provided rather than learned from the offline dataset as in D4RL tasks; and the dataset (for offline RL) does not include the reference shot or any nearby, similar shots.

E. Additional Evaluation Results

In this section, we provide additional empirical results to supplement the main findings presented in Section 5. The content is organized as follows: a quantitative and qualitative analysis of the benefits of belief adaptations in Section E.1, a comparison with model-free offline RL methods in Section E.2, an ablation study highlighting the necessity of incorporating the reward penalty in Section E.3, a comparison of our algorithm with leading offline RL baselines in Section E.4, and a detailed comparison with MuZero and its variants in terms of algorithm design, empirical performance, and computational cost in Section E.5.

E.1. Analysis of the Benefits of Belief Adaptation

hc-med-expert	hc-med-replay	hc-medium	hc-random
0.7515	2.6315	2.2674	2.4561
hp-med-expert	hp-med-replay	hp-medium	hp-random
14.064	4.2214	3.5913	1.7400
wk-med-expert	wk-med-replay	wk-medium	wk-random
2.0898	3.8169	34.264	1.0341

Table 6. Ratios of average transition likelihoods in offline data with and without belief adaptation across ensemble members. Bayesian belief adaptation based on observed transitions generally enhances prediction performance in the offline dataset, with the exception of hc-med-expert (i.e., the HalfCheetah dataset with medium-expert performance).

Data Type	Environment	Prediction Error on Next State		Prediction Error on Reward		Overall Prediction Error	
		Adaptive	Uniform	Adaptive	Uniform	Adaptive	Uniform
random	HalfCheetah	0.339 ± .021	0.342 ± .017	0.016 ± .001	0.016 ± .001	0.177 ± .011	0.179 ± .009
random	Hopper	0.232 ± .016	0.189 ± .008	0.012 ± .001	0.022 ± .008	0.122 ± .008	0.106 ± .008
random	Walker2d	62.10 ± 11.0	112.0 ± 19.0	1.364 ± .215	4.908 ± .708	31.73 ± 5.61	58.44 ± 9.83
medium	HalfCheetah	1.387 ± .040	1.355 ± .038	0.057 ± .001	0.061 ± .001	0.722 ± .021	0.708 ± .019
medium	Hopper	0.429 ± .033	0.570 ± .035	19.03 ± 8.58	68.24 ± 11.4	9.727 ± 4.30	34.40 ± 5.69
medium	Walker2d	34.01 ± .556	34.26 ± .142	24.38 ± 4.31	113.1 ± 3.47	29.19 ± 1.89	73.69 ± 1.78
med-replay	HalfCheetah	0.677 ± .027	0.707 ± .036	0.115 ± .005	0.114 ± .006	0.396 ± .016	0.410 ± .021
med-replay	Hopper	0.170 ± .022	0.212 ± .054	1.177 ± .420	3.320 ± 1.14	0.674 ± .221	1.766 ± .558
med-replay	Walker2d	66.83 ± 7.39	44.61 ± 1.34	27.21 ± 3.24	60.52 ± 3.17	47.02 ± 5.17	52.57 ± 2.25
med-expert	HalfCheetah	1.423 ± .054	1.467 ± .046	0.071 ± .002	0.074 ± .002	0.747 ± .028	0.771 ± .024
med-expert	Hopper	3.665 ± 2.56	18.27 ± 2.09	71.46 ± 79.9	384.7 ± 37.6	37.56 ± 41.2	201.5 ± 19.4
med-expert	Walker2d	55.69 ± 3.71	51.89 ± .481	121.9 ± 12.6	186.3 ± 3.86	88.77 ± 8.18	119.1 ± 2.08

Table 7. Comparison of the prediction errors for next states and rewards in imaginary rollouts, with and without Bayesian belief adaptation. The last two columns present the average prediction errors for next states and rewards, serving as an overall indicator. Each metric is computed over three repetitions with different random seeds, reporting both the mean and standard deviation. Ground truth for the imaginary rollouts is obtained by replaying the action sequences in the real simulators.

The Bayesian adaptation, as defined in Eq. (4), uses observed state transition sequences to adjust the belief over each

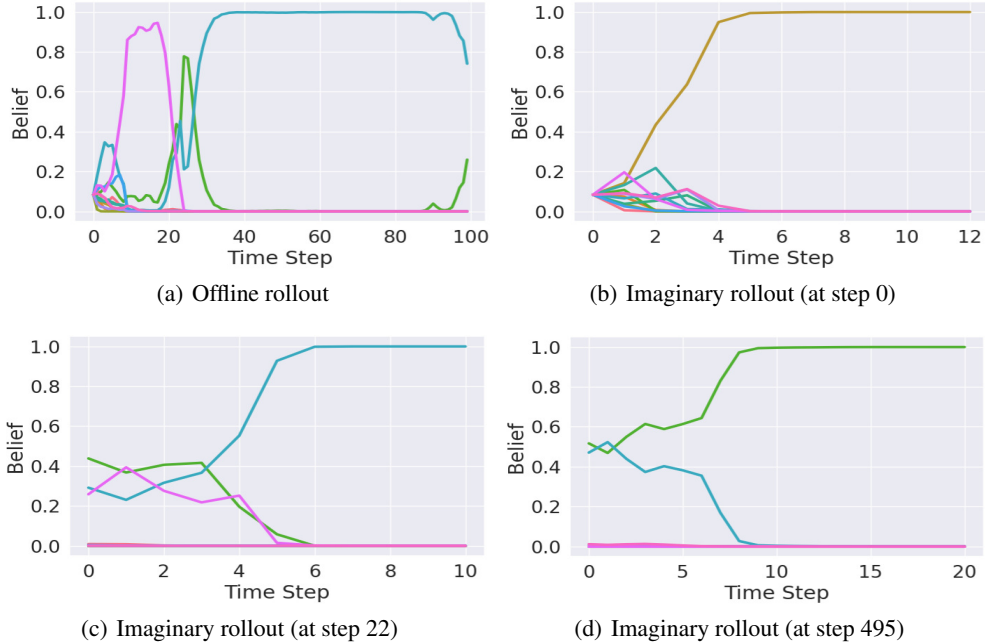


Figure 3. Belief adaptation during offline and imaginary rollouts. (a) shows the belief over twelve ensemble members, each represented by a specific color, adapting to an offline trajectory of Hopper-med-expert. (b), (c), and (d) illustrate the belief changes during imaginary rollouts which start from the beginning, middle, and end of the offline trajectory shown in (a), respectively.

ensemble member, thereby enhancing the quality of predicted rollout trajectories. For each benchmarking task in D4RL MuJoCo, we compute the average transition likelihood (i.e., $\mathcal{P}(s'|s, a)\mathcal{R}(r|s, a)$) for the provided offline rollouts (i.e., transitions like (s, a, r, s')), comparing cases with and without belief adaptation. The ratios of these likelihoods (averaged over all transitions in the offline dataset) are presented in Table 6. Results show that the offline rollouts, collected from real environments, are more likely under the adapted ensemble, with the exception of HalfCheetah-med-expert. This also demonstrates that Bayesian belief adaptation serves as an effective calibration method for the learned world models.

As detailed in Appendix C, at each learning epoch, we randomly sample states from the offline dataset to serve as starting points for imaginary rollouts, which are generated using the learned dynamics models. Belief adaptation is applied not only to the offline trajectories (to establish prior beliefs at these starting states) but also throughout the imaginary rollouts. To evaluate the quality of the imaginary rollouts, we select 10000 starting states from the offline dataset and perform rollouts using the same ensemble and behavior policy (based on MCTS), with the only difference being whether belief adaptation is applied to the ensemble members. Table 7 presents the prediction errors, measured as the average mean squared errors across each time step in the rollouts, for next states and rewards in the imaginary rollouts. Ground truth rollouts are generated by replaying the planned action sequences in the real simulators. The last two columns, which show the average prediction errors for next states and rewards, reveal that the adaptive ensemble achieves more accurate predictions in 10 out of 12 benchmarking tasks, with comparable performance in the remaining two.

Regarding the overall prediction error in Table 7, the adaptive ensemble significantly outperforms the uniform ensemble in Hopper-med-expert. To illustrate this, we plot the belief adaptation over an offline trajectory in Hopper-med-expert in Figure 3(a). Initially, all twelve ensemble members have the same belief. As the trajectory progresses, the beliefs of each member are updated based on the transition history, with the dominant model (the one with the highest belief) continuously changing. Additionally, we track the belief changes in imaginary rollouts starting from the beginning, middle, and end of the offline trajectory. It is evident that different ensemble members dominate at different stages of the offline rollout. This dynamic belief adaptation is crucial for achieving lower prediction errors during imaginary rollouts, as shown in Table 7.

Bayes Adaptive Monte Carlo Tree Search for Offline Model-based Reinforcement Learning

Data Type	Environment	BA-MCTS -SL (ours)	BA-MCTS (ours)	BA-MBRL (ours)	CQL	BEAR	BRAC-v	SAC	BC
random	HalfCheetah	29.20 ± 2.00	36.23 ± 1.04	32.76 ± 1.16	35.4	25.1	31.2	30.5	2.1
random	Hopper	33.83 ± 0.10	31.56 ± 0.12	31.47 ± 0.03	10.8	11.4	12.2	11.3	1.6
random	Walker2d	21.89 ± 0.07	21.59 ± 0.32	21.45 ± 0.53	7.0	7.3	1.9	4.1	9.8
medium	HalfCheetah	70.47 ± 3.52	75.84 ± 3.81	56.54 ± 5.20	44.4	41.7	46.3	-4.3	36.1
medium	Hopper	97.75 ± 7.09	96.70 ± 14.0	98.25 ± 3.42	86.6	52.1	31.1	0.8	29.0
medium	Walker2d	82.24 ± 1.85	74.73 ± 3.25	75.41 ± 4.17	74.5	59.1	81.1	0.9	6.6
med-replay	HalfCheetah	61.16 ± 1.60	65.45 ± 0.81	62.50 ± 0.18	46.2	38.6	47.7	-2.4	38.4
med-replay	Hopper	106.3 ± 0.13	101.8 ± 3.46	93.91 ± 4.25	48.6	33.7	0.6	3.5	11.8
med-replay	Walker2d	92.13 ± 5.13	95.06 ± 2.11	97.54 ± 1.93	32.6	19.2	0.9	1.9	11.3
med-expert	HalfCheetah	80.53 ± 6.63	76.16 ± 10.3	90.52 ± 4.13	62.4	53.4	41.9	1.8	35.8
med-expert	Hopper	112.2 ± 0.29	108.3 ± 0.22	107.8 ± 0.37	111	96.3	0.8	1.6	111.9
med-expert	Walker2d	107.7 ± 0.82	110.0 ± 1.74	84.71 ± 0.87	98.7	40.1	81.6	-0.1	6.4
Average Score		74.62	74.45	71.06	54.85	39.83	31.44	4.13	25.07

Table 8. Comparisons between the proposed algorithms and model-free offline policy learning methods on the D4RL benchmark suite. Each value represents the normalized score, as proposed in (Fu et al., 2020), of the policy trained by the corresponding algorithm. These scores are undiscounted returns normalized to approximately range between 0 and 100, where a score of 0 corresponds to a random policy and a score of 100 corresponds to an expert-level policy. For our algorithms, we report the average score of the final ten policy learning epochs and its standard deviation across three different random seeds.

E.2. Comparison with Model-free Methods on D4RL MuJoCo

As a complement to Table 1, we compare our algorithms with a series of model-free offline policy learning (Chen et al., 2024b) methods. We include SOTA model-free offline RL methods: CQL (Kumar et al., 2020), BEAR (Kumar et al., 2019), and BRAC-v (Wu et al., 2019). Additionally, we show the performance of directly applying SAC or Behavioral Cloning (BC) (Chen et al., 2024b) to the provided offline dataset in the last two columns. The mean performance of the baselines are taken from related works (Yu et al., 2020; Kidambi et al., 2020; Fu et al., 2020). Our algorithms show significantly better performance, demonstrating the necessity of model-based learning in these environments. The training plots of our proposed algorithms in each environment is further detailed in Figure 4.

E.3. Ablation Study on the Reward Penalty

Data Type	Environment	BA-MCTS -SL	BA-MCTS	BA-MBRL	BA-MCTS -SL ($\lambda = 0$)	BA-MCTS ($\lambda = 0$)	BA-MBRL ($\lambda = 0$)
random	HalfCheetah	29.20 ± 2.00	36.23 ± 1.04	32.76 ± 1.16	34.80 ± 1.39	38.78 ± 1.65	39.64 ± 2.86
random	Hopper	33.83 ± 0.10	31.56 ± 0.12	31.47 ± 0.03	9.16 ± 0.16	7.44 ± 0.14	6.97 ± 0.07
random	Walker2d	21.89 ± 0.07	21.59 ± 0.32	21.45 ± 0.53	17.53 ± 6.16	21.53 ± 0.42	21.41 ± 0.64
medium	HalfCheetah	70.47 ± 3.52	75.84 ± 3.81	56.54 ± 5.20	61.64 ± 4.58	60.84 ± 2.00	41.49 ± 2.29
medium	Hopper	97.75 ± 7.09	96.70 ± 14.0	98.25 ± 3.42	102.8 ± 2.29	104.4 ± 1.88	93.68 ± 11.4
medium	Walker2d	82.24 ± 1.85	74.73 ± 3.25	75.41 ± 4.17	82.61 ± 0.86	57.01 ± 7.24	57.97 ± 15.4
med-replay	HalfCheetah	61.16 ± 1.60	65.45 ± 0.81	62.50 ± 0.18	42.10 ± 2.85	36.65 ± 2.39	44.03 ± 7.35
med-replay	Hopper	106.3 ± 0.13	101.8 ± 3.46	93.91 ± 4.25	107.9 ± 0.07	84.11 ± 2.97	91.81 ± 11.5
med-replay	Walker2d	92.13 ± 5.13	95.06 ± 2.11	97.54 ± 1.93	88.61 ± 5.21	97.33 ± 3.51	98.19 ± 1.23
med-expert	HalfCheetah	80.53 ± 6.63	76.16 ± 10.3	90.52 ± 4.13	51.76 ± 5.31	26.60 ± 1.46	29.88 ± 2.28
med-expert	Hopper	112.2 ± 0.29	108.3 ± 0.22	107.8 ± 0.37	106.8 ± 6.34	81.76 ± 6.45	86.79 ± 18.7
med-expert	Walker2d	107.7 ± 0.82	110.0 ± 1.74	84.71 ± 0.87	110.8 ± 1.72	110.2 ± 0.91	53.35 ± 38.0
Average Score		74.62	74.45	71.06	68.04	60.55	55.43

Table 9. Comparison of the proposed algorithms with their corresponding versions without the reward penalty (i.e., $\lambda = 0$). The definitions of the scores in this table are consistent with those in Table 8.

To demonstrate the necessity of incorporating the reward penalty in offline MBRL, we conduct an ablation study by setting λ in Eq. (5) to 0, resulting in ablated versions of our proposed three algorithms. The results are presented in Table 9. **First**, the average performance of the algorithms with the reward penalty is consistently better, demonstrating the importance of using reward penalties in offline MBRL to prevent the overexploitation of the learned world models (which can be inaccurate). **Second**, the supervised-learning-based algorithm (i.e., BA-MCTS-SL ($\lambda = 0$)) is less affected by the absence of the reward penalty, compared to the policy-gradient-based methods. Notably, BA-MCTS-SL ($\lambda = 0$) and BA-MCTS-SL achieve

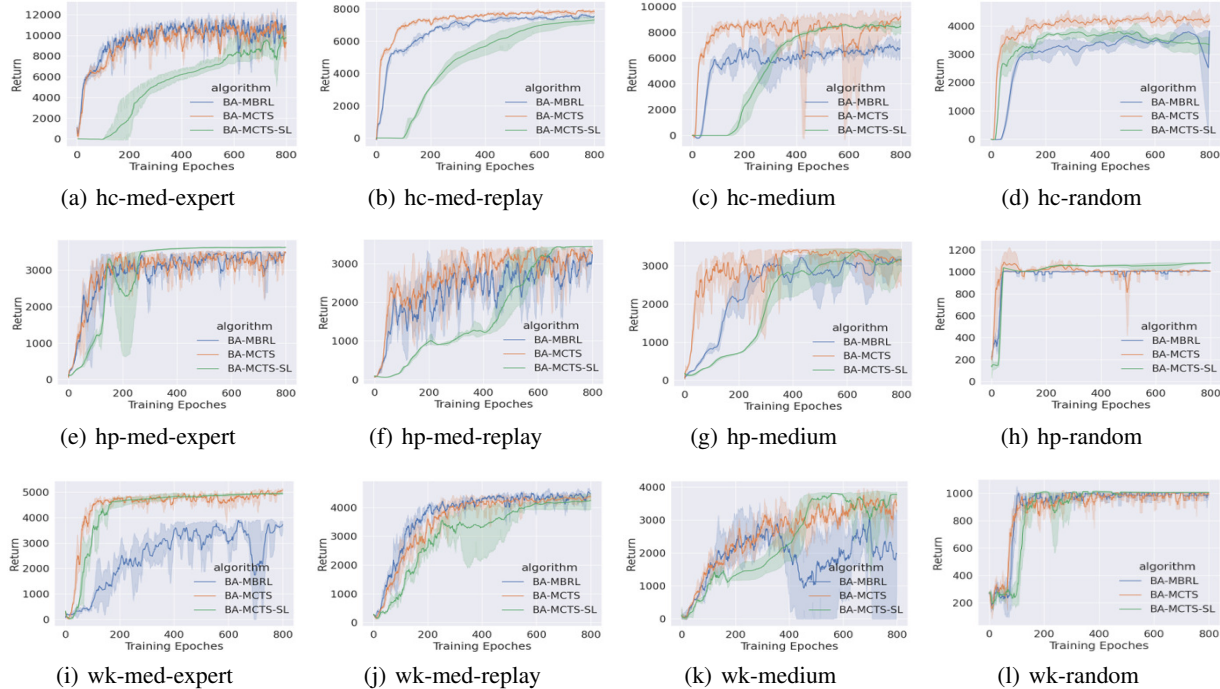


Figure 4. Performance of our proposed algorithms on D4RL MuJoCo tasks. The results for HalfCheetah, Hopper, and Walker2d are presented in the three rows, respectively. Each subfigure depicts the change in the undiscounted episodic return as a function of training epochs. Experiments are repeated three times with different random seeds, with the solid line representing the mean and the shaded area indicating the 95% confidence interval. For reference, the expert-level episodic returns for HalfCheetah, Hopper, and Walker2d are 12135, 3234.3, and 4592.3, respectively. Note that the training epochs for each algorithm, as listed in Table 3, have been linearly scaled to 800 for better visualization.

comparable performance in the Hopper and Walker2d tasks. This shows an additional advantage of BA-MCTS-SL – its reduced sensitivity to model inaccuracies. **Lastly**, there are instances where superior performance is achieved with λ set to 0. For example, BA-MCTS-SL ($\lambda = 0$) performs better than BA-MCTS-SL in 5 out of 12 tasks. This suggests that the performance of our algorithms in Tables 1 and 8 could be further improved by adjusting hyperparameters such as λ ⁹.

E.4. Comparison with Leading Offline RL Baselines

As noted in Section 5, the implementation of our algorithms is based on Optimized, making minimal changes to its codebase and hyperparameter settings. Therefore, the performance improvements shown in Table 1 stem from the Bayesian RL framework and deep search components. Our algorithms can be seamlessly integrated with other advancements in offline MBRL, such as RNN-based policy functions, more accurate world model learning, and improved uncertainty quantification.

To testify this, we replace the reward penalty design in Eq. (5) with the one proposed in a recent work (Sun et al., 2023). Specifically, this reward penalty measures the discrepancy in the Q-value targets of the next states predicted by each ensemble member. It is calculated based not only on the ensemble but also on the target Q network and policy network:

$$\tilde{r}(s, a, r) = r - \lambda \cdot \text{std} \left[\frac{\gamma}{M} \sum_{j=1}^M Q_{\psi^-}(s'_{i,j}, a'_{i,j}) \right]_{i=1}^K, \quad s'_{i,j} \sim \mathcal{P}_{\theta^i}(\cdot|s, a), \quad a'_{i,j} \sim \pi(\cdot|s'_{i,j}) \quad (7)$$

Here, $(s'_{i,j}, a'_{i,j})$ are samples generated from the learned dynamics and policy models. These samples are fed into the target Q network, Q_{ψ^-} , to estimate the Q-value target for the current state-action pair (s, a) . The reward penalty is computed as the standard deviation of the estimated Q-value targets across different ensemble members.

⁹As mentioned in Section 5, we retain most of the hyperparameter settings from Optimized (Lu et al., 2022) to ensure that the performance improvements are attributed to our algorithm design.

Bayes Adaptive Monte Carlo Tree Search for Offline Model-based Reinforcement Learning

Data Type	Environment	BA-MCTS (ours)	MOBILE	CBOP	RAMBO	APE-V	MAPLE
random	HalfCheetah	41.45 ± 1.40	39.27 ± 1.38	32.8	40.0	29.9	41.5
random	Hopper	31.42 ± 0.10	7.965 ± 0.43	31.4	21.6	31.3	10.7
random	Walker2d	21.54 ± 0.06	21.47 ± 0.03	17.8	11.5	15.5	22.1
medium	HalfCheetah	77.31 ± 1.40	76.42 ± 1.00	74.3	77.6	69.1	48.5
medium	Hopper	103.9 ± 0.33	102.5 ± 1.77	102.6	92.8	-	44.1
medium	Walker2d	88.23 ± 0.78	87.12 ± 2.79	95.5	86.9	90.3	81.3
med-replay	HalfCheetah	71.24 ± 2.65	64.67 ± 8.14	66.4	68.9	64.6	69.5
med-replay	Hopper	106.4 ± 0.53	105.7 ± 1.56	104.3	96.6	98.5	85.0
med-replay	Walker2d	91.42 ± 1.54	85.12 ± 10.1	92.7	85.0	82.9	75.4
med-expert	HalfCheetah	102.3 ± 2.27	100.9 ± 4.00	105.4	93.7	101.4	55.4
med-expert	Hopper	111.8 ± 0.82	111.9 ± 0.34	111.6	83.3	105.7	95.3
med-expert	Walker2d	116.0 ± 1.49	115.0 ± 0.30	117.2	68.3	110.0	107.0
Average Score		80.25	76.50	79.33	68.85	72.65	61.32

Table 10. Comparison of BA-MCTS with leading offline RL baselines on the D4RL benchmark suite. Each value in the table represents the normalized score as defined in Tables 1 and 8. Baseline results are sourced from their respective papers: CBOP (Jeong et al., 2023), RAMBO (Rigter et al., 2022), APE-V (Ghosh et al., 2022), and MAPLE (Chen et al., 2021). For BA-MCTS, enhanced performance is achieved by using the reward penalty design proposed in MOBILE (Sun et al., 2023). **For a fair comparison, we run BA-MCTS and MOBILE using the same ensemble of world models and identical hyperparameter settings, repeating each experiment three times with random seeds 0, 1, and 2. Additionally, we executed the publicly available code for CBOP from (Jeong et al., 2023) on the same set of tasks, using identical random seeds as our algorithm, but observed results that differed from those reported in (Jeong et al., 2023). Specifically, the performance for each task, corresponding to each row, is as follows: 32.95 ± 0.14 , 23.79 ± 11.2 , 1.391 ± 0.06 , 69.98 ± 0.88 , 98.68 ± 2.30 , 93.92 ± 1.92 , 63.36 ± 0.47 , 101.3 ± 1.74 , 74.56 ± 1.29 , 97.71 ± 5.26 , 111.2 ± 0.77 , 117.6 ± 0.27 . This yields a mean performance of 73.87.** The results of BA-MCTS, MOBILE, and CBOP are reproducible with our provided codebase.

With this modification, BA-MCTS achieves improved performance in several environments (compared to Table 1), and demonstrates state-of-the-art (SOTA) overall performance on the D4RL MuJoCo benchmark. Among the baselines in Table 10, APE-V and MAPLE employ adaptive policies implemented with RNNs¹⁰, while RAMBO, CBOP, and MOBILE are more recent baselines. Comparing BA-MCTS to these leading baselines showcases its SOTA performance. Note that, for a fair comparison, the same ensemble of world models and hyperparameter setup (published by (Sun et al., 2023)) are used for BA-MCTS and MOBILE.

E.5. Comparison with MuZero and its Variants

Monte-Carlo Tree Search (MCTS) (Browne et al., 2012) has been successfully integrated with RL, as exemplified by AlphaZero (Silver et al., 2017a) and MuZero (Schrittwieser et al., 2020). These methods have achieved superhuman performance in domains requiring highly sophisticated decision-making processes. AlphaZero relies on given world models, whereas MuZero learns the world model and policy simultaneously by interacting with the environment. Although there have been various extensions of MuZero (Hubert et al., 2021; Schrittwieser et al., 2021; Ye et al., 2021; Antonoglou et al., 2022; Oren et al., 2022; Zhao et al., 2024), most algorithms are designed for online MBRL. According to (Niu et al., 2023), the applications of MuZero in offline learning, especially for continuous control in highly stochastic environments, which is our focus, still require significant improvement. **Our algorithm design differs from MuZero (and its variants) in several key aspects: (1) MuZero integrates model learning and policy training into a single stage, using a world model defined in a latent state space. Our algorithm separately learns a world model and then trains the policy on top of it, aligning with the widely-adopted offline MBRL framework. (2) MuZero employs a single latent world model (rather than an ensemble) and does not explicitly account for uncertainty in dynamics or reward predictions. This makes it particularly vulnerable to modeling errors in offline MBRL. (3) We introduce double progressive widening (Auger et al., 2013) and Bayes-adaptive planning into MCTS, resulting in a fundamentally different planning algorithm compared to the one used in MuZero.**

As noted in Section 5.2, we select a state-of-the-art variant of MuZero, i.e., Sampled EfficientZero, as a baseline and test its performance on the D4RL MuJoCo tasks. The evaluation results are presented in Figure 1. For reference, the expert-level episodic returns (corresponding to scores of 100) for HalfCheetah, Hopper, and Walker2d are 12135, 3234.3, and 4592.3,

¹⁰APE-V is a model-free algorithm, and MAPLE does not utilize a Bayesian RL framework, making their algorithm designs fundamentally different from ours.

respectively. Thus, the results are significantly worse compared to the performance of offline RL methods listed in Table 1, despite Sampled EfficientZero’s higher computational cost.

Data Type	Environment	BA-MCTS -SL (ours)	BA-MCTS (ours)	BA-MBRL (ours)	Sampled EfficientZero
random	HalfCheetah	11.2 ± 2.6	14.6 ± 2.2	1.2 ± 0.4	54.8 ± 2.6
random	Hopper	48.7 ± 2.4	65.2 ± 1.9	5.6 ± 0.8	153.7 ± 19.4
random	Walker2d	25.7 ± 2.0	38.1 ± 1.1	5.2 ± 1.1	175.7 ± 28.2
medium	HalfCheetah	12.6 ± 3.0	15.3 ± 1.3	1.9 ± 0.2	54.7 ± 1.9
medium	Hopper	18.9 ± 4.8	67.5 ± 0.2	1.8 ± 0.2	70.5 ± 1.0
medium	Walker2d	24.0 ± 1.8	33.3 ± 4.0	4.8 ± 1.0	63.7 ± 1.5
med-replay	HalfCheetah	24.7 ± 0.9	22.4 ± 1.2	2.1 ± 0.4	54.8 ± 1.8
med-replay	Hopper	17.9 ± 0.0	12.7 ± 1.2	5.4 ± 0.2	126.6 ± 12.0
med-replay	Walker2d	40.3 ± 7.2	77.0 ± 2.4	8.0 ± 0.3	134.9 ± 4.2
med-expert	HalfCheetah	32.6 ± 0.1	12.6 ± 0.8	4.7 ± 1.1	55.4 ± 1.3
med-expert	Hopper	61.5 ± 4.6	76.9 ± 11.6	5.3 ± 0.5	66.1 ± 0.9
med-expert	Walker2d	35.0 ± 6.5	55.9 ± 1.8	2.9 ± 0.9	60.8 ± 1.8

Table 11. Training time (in hours) of the proposed algorithms and Sampled EfficientZero for each evaluation task. Results are presented as the mean and standard deviation from three repeated experiments.

In Table 11, we report the training time of the proposed algorithm and Sampled EfficientZero on the D4RL MuJoCo tasks. The experiments were conducted on a server with 40 Intel(R) Xeon(R) Gold 5215 CPUs and 4 Tesla V100-SXM2-32GB GPUs. While the tree-search-based variants (i.e., BA-MCTS and BA-MCTS-SL) achieve higher performance, they require more computation during the offline training stage than BA-MBRL. However, this extra computational cost is limited to the training phase; no MCTS is performed during deployment, to ensure real-time execution. Additionally, leveraging parallel computation frameworks for MCTS could further reduce the training time. On the other hand, our algorithm requires considerably less training time than Sampled EfficientZero, which is also based on deep search, to achieve superior performance, as shown in Figures 1 and 4.